[AMERICAN JOURNAL OF SCIENCE, VOL. 278, MAY, 1978, P. 638-686]

CALCULATION OF THE THERMODYNAMIC CONSEQUENCES OF DEHYDRATION IN SUBDUCTING OCEANIC CRUST TO 100 KB AND > 800°C

JOAN M. DELANY* and HAROLD C. HELGESON

Department of Geology and Geophysics,
University of California, Berkeley, California 94720

ABSTRACT. The thermodynamic properties of H_2O at pressures > 10 kb and temperatures to 800°C were computed from a fourth degree equation of state derived by regression of Gibbs free energies generated by Tödheide from Jüza's (1966) calculations of the density of H_2O at high pressures and temperatures. The equation was then combined with thermodynamic data for minerals to calculate equilibrium pressures and temperatures and the thermodynamic properties of invariant and univariant dehydration reactions in the system CaO–MgO–Na_2O–K_2O–Al_2O_3–SiO_2–H_2O to 100 kb. Correlation of the calculations with compositional and thermal models of descending plates indicates that such reactions may contribute significantly to both geochemical and geophysical processes in subducting oceanic crust at depths $\lesssim$ 150 km. Univariant dehydration curves commonly exhibit temperature extrema at $\sim$ 5 to 25 kb in response to changes in the volumetric properties of H_2O, which in many cases lead to relatively small negative Clapeyron slopes at high pressures and low temperatures. Dehydration reactions are endothermic ($\Delta H° \approx$ 2 to 19 kcal (mole H_2O)$^{-1}$) and exhibit negative volume changes of the order of 5 percent at high pressures, which favor generation of earthquakes and local depression of geothermal gradients in subduction zones. The fugacity of H_2O, which increases with pressure, is of the order of 10^{11} bars at 100 kb. Liberation of H_2O may thus exert a catalytic influence on reaction rates and melting of mantle material. Calculation of the thermodynamic consequences of dehydration in subducting oceanic crust affords a petrogenetic grid for metamorphic facies at high pressures and provides a quantitative basis for assessing the impact of such reactions on the distribution of temperature in descending plates.

INTRODUCTION

Developments in plate tectonic theory leave little doubt that significant quantities of H_2O are liberated in the upper mantle by dehydration of serpentine, talc, amphiboles, and other hydrous minerals in the oceanic crust of downgoing slabs. Although dehydration of these minerals at depth has received considerable attention, the thermodynamic consequences of the process are still poorly understood. The purpose of this communication is to evaluate these consequences by calculating and comparing the thermodynamics of dehydration reactions in subducting plates at pressures and temperatures corresponding to those in the upper mantle.

Most experimental investigations of phase equilibria at high temperatures and pressures > 10 kb are concerned with melting relations and solid/solid phase transitions (Green and Ringwood, 1967a, b; Akimoto and Fugisawa, 1968; Kushiro, 1970; Huang and Wyllie, 1975; Ming and Bassett, 1975; Ringwood, 1972; Ringwood and Major, 1967a; Green, 1973; Nicholls and Ringwood, 1973a, b; Lambert and Wyllie, 1968, 1970a; Hill and Boettcher, 1970; Chen and Presnall, 1975; Mysen and Boettcher, 1975; and others). With a few notable exceptions (for example, Essene,

* Present address: Department of Earth and Space Sciences, University of California, Los Angeles, California 90024

Hensen, and Green, 1970; Allen and others, 1972) comparable studies of dehydration reactions at high pressures have focused on phase relations in the systems Al_2O_3–H_2O, MgO–SiO_2–H_2O, and CaO–H_2O (Kitahara, Takenouchi, and Kennedy, 1966; Sclar and Carrison, 1966; Ringwood and Major, 1967b; Kennedy, 1959; Pistorius, 1963a, b; Yamaoka, Fukunaga, and Saito, 1970; Irving, Huang, and Wyllie, 1977; Yamamoto and Akimoto, 1974, 1977). Nevertheless, there seems to be general agreement that the oceanic crust consists largely of basalts and gabbros that have been hydrothermally altered and metamorphosed to greenschists and amphibolites (Christensen, 1970a, b, 1972; Ringwood, 1974, 1975; Melson, Thompson, and van Andel, 1968; Miyashiro, 1973; Spooner and Fyfe, 1973; Wolery and Sleep, 1976). As emphasized by Lambert and Wyllie (1970b), Hasebe, Fujii, and Uyeda (1970), Allen and others (1972), Wyllie (1970, 1971, 1973), Ringwood (1974), Fyfe and McBirney (1975), Anderson, Uyeda, and Miyashiro (1976), and others, dehydration of minerals in these altered rocks may contribute significantly to the mineralogic constitution of the upper mantle. Although equilibrium temperatures have been estimated for a number of dehydration reactions at high pressures (Kitahara and Kennedy, 1967; Wall and Essene, 1972; Essene, Wall, and Shettel, 1973), the thermodynamic properties of the reactions have yet to be evaluated. Recent progress in theoretical geochemistry permits calculation of these properties from a revised set of thermodynamic data for minerals (Helgeson, Delany, Nesbitt, and Bird, 1978) and an equation of state for H_2O at pressures and temperatures to 100 kb and > 800°C.

CONVENTIONS AND NOTATION

The standard state for solids and H_2O adopted in this study corresponds to unit activity of the pure component at any temperature and pressure. Standard Gibbs free energies and enthalpies of formation are expressed as apparent molal quantities, which are defined by (Benson, 1968; Helgeson, 1969; Helgeson and Kirkham, 1974, 1976)

$$\Delta G^\circ_{P,T,i} \equiv \Delta G^\circ_{f,i} + (G^\circ_{P,T,i} - G^\circ_{P_r,T_r,i}) \tag{1}$$

and

$$\Delta H^\circ_{P,T,i} \equiv \Delta H^\circ_{f,i} + (H^\circ_{P,T,i} - H^\circ_{P_r,T_r,i}) \tag{2}$$

where $\Delta G^\circ_{P,T,i}$ and $\Delta H^\circ_{P,T,i}$ stand for the apparent standard molal Gibbs free energy and enthalpy of formation of the ith species at the subscripted pressure (P) and temperature (T), $\Delta G^\circ_{f,i}$ and $\Delta H^\circ_{f,i}$ denote the standard molal Gibbs free energy and enthalpy of formation from the elements of the species at the reference pressure (P_r) and temperature (T_r) of 1 bar and 298.15°K, and the two parenthetical terms correspond, respectively, to the difference in the standard molal Gibbs free energy and enthalpy of the *species* at the pressure and temperature of interest and that at P_r, T_r.

Apparent standard molal enthalpies and Gibbs and Helmholtz free energies of formation are expressed in thermochemical calories (4.184 joules) or kilocalories mole^{-1} (cal mole^{-1} or kcal mole^{-1}), entropies and heat capacities in cal mole^{-1} (°K)$^{-1}$, and molal volumes in cm^3 mole^{-1} (which can be converted to cal mole^{-1} bar^{-1} by multiplying by 0.0239 cal cm^{-3} bar^{-1}). The activity of the ith component (a_i) and the equilibrium constant (K) are dimensionless, which requires activity coefficients to have reciprocal units of concentration. All thermodynamic properties of H_2O are consistent with those given by Helgeson and Kirkham (1974) for a molecular weight of 18.0153 gm mole^{-1}. Pressure is expressed in bars or kilobars (kb) and temperature in °C or °K.

SYMBOLS

$\Delta A°$	Apparent standard molal Helmholtz free energy of formation.
a_i	Activity of the ith component.
$a_{j\,l}$	Equation of state coefficients for H_2O at pressures and temperatures from 10^3 to 10^5 bars and 25° to 800°C.
$C°_{P_r}$	Standard molal heat capacity at the reference pressure (P_r).
$\Delta C_{P_r,r}$	Standard molal heat capacity of reaction at the reference pressure (P_r).
f_i	Fugacity of the ith component.
$\Delta G°$	Apparent standard molal Gibbs free energy of formation.
$\Delta G°_f$	Standard molal Gibbs free energy of formation from the elements at 298.15°K and 1 bar.
$\Delta G°_r$	Standard molal Gibbs free energy of reaction.
$\Delta H°$	Apparent standard molal enthalpy of formation.
$\Delta H°_f$	Standard molal enthalpy of formation from the elements at 298.15°K and 1 bar.
$\Delta H°_r$	Standard molal enthalpy of reaction.
i	Integer index ($i = 1, 2, \ldots \hat{\imath}$) designating components in a system or species in a reaction.
K	Equilibrium constant.
$\tilde{n}_i$	Stoichiometric reaction coefficient of the ith species in a chemical reaction.
P	Total pressure in bars or kb.
P_r	Reference pressure (1 bar).
R	Gas constant (1.9872 cal mole^{-1} (°K)$^{-1}$).
$S°$	Standard molal entropy.
$\Delta S°_r$	Standard molal entropy of reaction.
T	Temperature in °C or °K.
T_r	Reference temperature (298.15°K).
$V°$	Standard molal volume.
$\Delta V°_r$	Standard molal volume of reaction.
X_i	Mole fraction of the ith component.
λ_i	Activity coefficient of the ith component.

THEORETICAL CONSIDERATIONS

Reactions among minerals represented by ψ_i (where i designates a particular mineral) in equilibrium with H_2O can be written as

$$\sum_{i=1}^{\hat{i}-1} \tilde{n}_i \psi_i = \tilde{n}_{\hat{i}}\, H_2O \tag{3}$$

where $\tilde{n}_i$ stands for the stoichiometric reaction coefficient of the ith species, which is positive for products and negative for reactants. Note that in eq (3) $i = 1, 2, \ldots (\hat{i}-1)$ designates mineral components and $\hat{i}$ refers to H_2O. The standard molal Gibbs free energy change for reaction (3) at a given pressure and temperature ($\Delta G^\circ_{P,T,r}$) can be expressed as

$$\Delta G^\circ_{P,T,r} = \sum_{i=1}^{\hat{i}} \tilde{n}_i\, \Delta G^\circ_{P,T,i} = \sum_{i=1}^{\hat{i}-1} \tilde{n}_i\, \Delta G^\circ_{P,T,i} + \tilde{n}_{\hat{i}}\, \Delta G^\circ_{P,T,\hat{i}} \tag{4}$$

where $\Delta G^\circ_{P,T,i}$ stands for the apparent standard molal Gibbs free energy of formation of the ith species in the reaction. The dependence of the apparent standard molal Gibbs free energy of formation of the ith species (eq 1) on temperature and pressure is given by

$$G^\circ_{P,T,i} - G^\circ_{P_r,T_r,i} = -S^\circ_{P_r,T_r,i}(T - T_r) + \int_{T_r}^{T} C^\circ_{P_r,i}\,dT - T\int_{T_r}^{T} C^\circ_{P_r,i}\,d\,\ln T + \int_{P_r}^{P} V^\circ_{T,i}\,dP \tag{5}$$

which is consistent with

$$H^\circ_{P,T,i} - H^\circ_{P_r,T_r,i} = \int_{T_r}^{T} C^\circ_{P_r,i}\,dT + \int_{P_r}^{P}\left(V^\circ_{T,i} - T\left(\frac{\partial V^\circ_i}{\partial T}\right)_P\right) dP \tag{6}$$

and

$$S^\circ_{P,T,i} - S^\circ_{P_r,T_r,i} = \int_{T_r}^{T} C^\circ_{P_r,i}\,d\,\ln T - \int_{P_r}^{P}\left(\frac{\partial V^\circ_i}{\partial T}\right)_P dP \tag{7}$$

where $G^\circ_{P,T,i}$, $H^\circ_{P,T,i}$, $S^\circ_{P,T,i}$, $C^\circ_{P_r,i}$, and $V^\circ_{T,i}$ represent the standard molal Gibbs free energy, enthalpy, entropy, heat capacity, and volume of the ith species at the subscripted pressure and temperature.

Thermodynamics of minerals as a function of pressure and temperature.—The standard molal heat capacities of minerals can be expressed as a function of temperature at 1 bar by (Kelley, 1960)

$$C_{P_r,T,i} = a_i + b_i T + c_i T^{-2} \tag{8}$$

where a_i, b_i, and c_i are constants characteristic of the ith mineral. Although the standard molal volumes of solids are not strictly independent of temperature and pressure, it seems likely that $\sum_{i=1}^{i-1} \tilde{n}_i V^\circ_i$ varies only slightly over the temperature/pressure range considered in this study. Except for reactions involving only solids, slight changes in volume with pressure and temperature have a negligible effect on calculated equilibrium pressures and temperatures below ~ 10 to ~ 50 kb, depending on the reaction (Helgeson, Delany, Nesbitt, and Bird, 1978).

Few expansibility data are available for hydrous minerals other than pyrophyllite and tremolite, but changes in volume with increasing pressure of phlogopite, muscovite, hornblende, biotite, and epidote have been determined experimentally at 25°C and pressures to ~ 40 kb (Birch, 1966; Simmons and Wang, 1971). Unfortunately, the compositions of the minerals used in the latter experiments are not reported, which precludes definitive calculation of the effect of pressure on the volumes of the stoichiometric phases. However, elastic constants for anhydrous minerals are well known and afford a means to estimate the order of magnitude of the effects of increasing pressure and temperature on the thermodynamic properties of minerals involved in dehydration reactions.

Thermal expansion of minerals causes an increase in volume of the order of 2 to 3 percent or less as temperature increases from 20° to 800°C at 1 bar (Skinner, 1966; Cameron and others, 1973; Sueno and others, 1973; Finger and Ohashi, 1976). However, a 3 percent increase in volume due to thermal expansion corresponds to the decrease in volume exhibited by minerals as pressure increases to 15 to 40 kb at 25°C, depending on the mineral (Birch, 1966). Expansibility and compressibility data at high pressures and temperatures are available only for simple compounds, but those reported by Birch (1966), Spetzler (1970), Spetzler, Sammis, and O'Connell (1972), and others, together with lattice model calculations (for example, see Demarest, 1972), suggest that the isothermal bulk modulus of minerals may decrease by as much as an order of magnitude as temperature increases to ~ 1000°C. It thus appears that the effects of thermal expansion on the standard molal volumes of minerals are essentially offset by the effects of compressibility at high pressures and temperatures. For this reason, and because the compressibilities and expansibilities of minerals decrease with increasing pressure (Birch, 1966; Skinner, 1966), calculation of the thermodynamic properties of dehydration reactions at high temperatures and pressures assuming $V^\circ_{P,T,i}$ for minerals to be equal to $V^\circ_{1\ bar,\ 298.15^\circ K,i}$ probably leads to small errors at pressures from 1 to $\sim 10^5$ bars. In the lower part of this range the net contribution of thermal expansion and compressibility to ΔG°_i for minerals is positive, but at higher pressures it becomes negative.

In addition to the partial compensation of the effects of $(\partial V^\circ_i/\partial P)_T$ and $(\partial V^\circ_i/\partial T)_P$ on ΔG°_i for minerals at high pressures and temperatures, the respective contributions of the thermal expansions and compressibilities of minerals to $\Delta V^\circ_{P,T,r}$ tend to cancel, even in the case of dehydration reactions. For example, expansibility and volume data taken from Cameron and others (1973), Sueno and others (1973), Skinner (1966), and Robie and Waldbaum (1968) for tremolite and its dehydration products indicate that the sum of $\tilde{n}_i(\partial V^\circ_i/\partial T)_P$ for 2 diopside + 3 enstatite + α-quartz is approximately equal to $(\partial V^\circ_i/\partial T)_P$ of tremolite (9.6×10^{-3} cm^3 mole^{-1} (°K)$^{-1}$) at $\sim$ 500°C and 1 bar (Helgeson, Delany, Nesbitt, and Bird, 1978). At other pressures and temperatures the difference is finite but certainly negligible compared to $(\partial V^\circ_i/\partial T)_P$ of H_2O. Owing to the opposing effects of V°_i and $(\partial V^\circ_i/\partial T)_P$ on the standard molal enthalpies of minerals as a function of pressure, errors in $\Delta H^\circ_{P,T,i}$ caused by the constant volume assumption should be smaller than corresponding errors in $\Delta G^\circ_{P,T,i}$.

The observations summarized above lead to the conclusion that errors introduced by the approximation

$$V^\circ_{P,T,i} = V^\circ_{P_r,T_r,i} \tag{9}$$

are unlikely to exceed half a cal mole^{-1} (°K)$^{-1}$ in ΔS°_r and a few hundred cal mole^{-1} in ΔH°_r and ΔG°_r at pressures and temperatures $\lesssim$ 100 kb and 800°C. The effect of this order of magnitude of uncertainty on prediction of equilibrium temperatures for a given dehydration reaction at high pressures can be assessed by first writing (Helgeson, Delany, Nesbitt, and Bird, 1978).

$$\delta T = \frac{\delta \Delta H^\circ_r - T\,\delta \Delta S^\circ_r}{\Delta S^\circ_r} \tag{10}$$

where δ designites finite difference derivatives. Uncertainties in ΔH°_r and ΔS°_r of $\sim$ 300 cal mole^{-1} and $\sim$ 0.5 cal mole^{-1} (°K)$^{-1}$ at 800°C caused by omitting provision for the thermal expansion and compression of minerals in computing ΔG°_r will thus introduce uncertainties in equilibrium temperatures of the order of a few tens of degrees or less if ΔS°_r is $\sim$ 10 cal mole^{-1} (°K)$^{-1}$ or more, which is the case for many dehydration reactions (see below). However, because ΔS°_r is commonly $<$ 5 cal mole^{-1} (°K)$^{-1}$ for reactions involving only solids, errors introduced by eq (9) may seriously affect predicted equilibrium temperatures and pressures for such reactions.

Eqs (8) and (9) permit evaluation of the integrals in eqs (5) through (7), which leads to

$$\begin{aligned} G^\circ_{P,T,i} - G^\circ_{P_r,T_r,i} = &- S^\circ_{P_r,T_r,i}\,(T - T_r) \\ &+ a_i\,(T - T_r - T\,ln\,(T/T_r)) \\ &- \frac{(b_i T\,T_r^2 + c_i)\,(T - T_r)^2}{2T_r^2 T} \\ &+ V^\circ_{P_r,T_r,i}\,(P - P_r), \end{aligned} \tag{11}$$

$$H^\circ_{P,T,i} - H^\circ_{P_r,T_r,i} = a_i (T - T_r) + \frac{b_i}{2} (T^2 - T_r^2) - c_i \left(\frac{1}{T} - \frac{1}{T_r}\right) + V^\circ_{P_r,T_r,i} (P - P_r), \quad (12)$$

and

$$S^\circ_{P,T,i} - S^\circ_{P_r,T_r,i} = a_i \ln (T/T_r) + b_i (T - T_r) - \frac{c_i}{2}\left(\frac{1}{T^2} - \frac{1}{T_r^2}\right). \quad (13)$$

Eqs (1), (2), and (11) through (13) permit calculation of the apparent standard molal Gibbs free energies and enthalpies of formation and the standard molal entropies of minerals at high pressures and temperatures consistent with the approximation represented by eq (9). Although in certain cases the absolute errors introduced by this approximation in computing values of ΔG°_r, ΔH°_r, ΔS°_r, and ΔV°_r may be significant, their *relative* counterparts for a series of dehydration reactions should be slight at pressures and temperatures < 100 kb and 800°C.

Thermodynamic properties of H_2O at high pressures.—Extensive experimental investigation of densities in the system H_2O (fig. 1) has led to a number of reliable and comprehensive equations of state for pressures < 10 kb (for example, Keenan and others, 1969; Burnham, Holloway, and Davis, 1969; Helgeson and Kirkham, 1974). Corresponding compilations and equations for higher pressures (Rice and Walsh, 1957; Pistorius and Sharp, 1960, 1961; Howard, 1961; Sharp, 1962; Kennedy and Holser, 1966; Jüza, 1966; Tödheide, 1972) are based primarily on early compressibility measurements (Bridgman, 1942) and shock wave data (Walsh and Rice, 1957). Gibbs free energy values computed by Tödheide (1972)

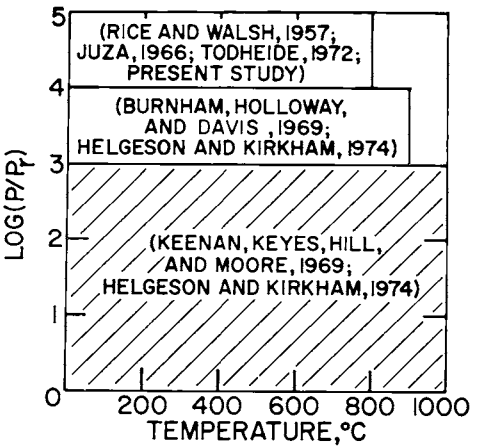

Fig. 1. Pressure/temperature regions considered in various experimental and theoretical studies of the thermodynamic properties of H_2O.

TABLE 1

Coefficients for eqs (15) through (17).

$a_{j\ell} = b_{j\ell} \times 10^{c_{j\ell}}$

j	ℓ = 0		ℓ = 1		ℓ = 2		ℓ = 3		ℓ = 4	
	$b_{j\ell}$	$c_{j\ell}$	$b_{j\ell}$	$c_{j\ell}$	$b_{j\ell}$	$c_{j\ell}$	$b_{j\ell}$	$c_{j\ell}$	$b_{j\ell}$	$c_{j\ell}$
0	-5.6130073	4	3.8101798	-1	-2.1167697	-6	2.0266445	-11	-8.3225572	-17
1	-1.5285559	1	1.3752390	-4	-1.5586868	-9	6.6329577	-15		
2	-2.6092451	-2	3.5988857	-8	-2.7916588	-14				
3	1.7140501	-5	-1.6860893	-11						
4	-6.0126987	-9								

from Jüza's (1966) modified van der Waals equation of state for H_2O were used in the present study to calculate values of $\Delta G^\circ_{P,T,\hat{i}}$ at pressures > 10 kb from

$$\Delta G^\circ_{P,T,\hat{i}} = \Delta G^\circ_{10^4,T,\hat{i}} + (G^\circ_{P,T,\hat{i}} - G^\circ_{10^4,T,\hat{i}}) \tag{14}$$

where $\Delta G^\circ_{10^4,T,\hat{i}}$ refers to the apparent standard molal Gibbs free energy of formation of H_2O (designated by the subscript $\hat{i}$) at 10 kb and the temperature of interest. The values of $\Delta G^\circ_{10^4,T,\hat{i}}$ employed in the calculations were computed from equations summarized by Helgeson and Kirkham (1974)[1]. The calculated values of $\Delta G^\circ_{P,T,\hat{i}}$ at high pressures are thus consistent with those generated from eq (1) with the aid of thermodynamic data for liquid H_2O at 25°C and 1 bar (Wagman and others, 1968) and the densities of H_2O at pressures < 10 kb reported by Keenan and others (1969) and Burnham, Holloway, and Davis (1969). Because $\Delta G^\circ_{\hat{i}}$ is a relatively simple monotonic function of pressure and temperature above 10 kb, the computed values of $\Delta G^\circ_{P,T,\hat{i}}$ can be represented by a 4th degree orthogonal polynominal, which can be written as

$$\Delta G^\circ_{P,T,\hat{i}} = \sum_{j=1}^{4} \sum_{l=1}^{4-j} a_{jl}\, T^j P^l \tag{15}$$

where $a_{j,l}$ represents an array of pressure/temperature-independent coefficients, P stands for pressure in bars, and T refers to temperature in °C. Regression of the values of $\Delta G^\circ_{P,T,\hat{i}}$ with eq (15) generated the fit coefficients in table 1. The regression data array is represented by the symbols in figures 2 and 3. Values of $\Delta G^\circ_{\hat{i}}$ computed from eq (15) are given in table 2 and shown as solid curves in the figures.

It can be seen in figures 2 and 3 that eq (15) closely represents the apparent standard molal Gibbs free energy of formation of H_2O at pressures > 10 kb. Incorporation in the data array of values of $\Delta G^\circ_{\hat{i}}$ reported by Helgeson and Kirkham (1974) for 7, 8, and 9 kb insured consistency of the regression results with their values of $\Delta G^\circ_{\hat{i}}$ at pressures < 10 kb. The maximum fit residual represented by the differences between the

[1] These calculations took account of the typographical errors in a number of the equations summarized by Helgeson and Kirkham (1974). The last term on the right side of eq (15) should read $C_r(\ln T)_\tau$, and T in eqs (30) through (43), (72), (92), and (93) given by Helgeson and Kirkham should be replaced by t to indicate °C.

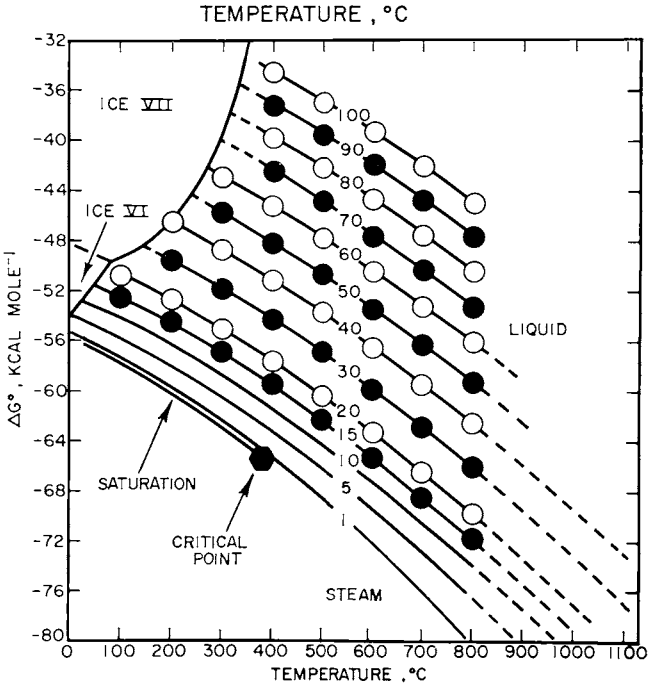

Fig. 2. Apparent standard molal Gibbs free energy of formation of H_2O (table 2) as a function of temperature at constant pressure (labeled in kb) computed (curves) from eq (15) and the coefficients in table 1 for pressures > 10 kb. The curves for pressures $\leq$ 10 kb were generated with the aid of equations given by Helgeson and Kirkham (1974). The symbols represent values calculated from Gibbs free energies computed by Tödheide (1972) using densities generated from Jüza's (1966) equation of state for H_2O (see text). The pressures and temperatures corresponding to the ice VI/VII transition and the melting curves for ice VI and VII are those reported by Brown and Whalley (1966) and Pistorius and others (1963).

curves and symbols in figures 2 and 3 is $\sim$ 100 cal mole^{-1}, but the bulk of the residuals are of the order of 50 cal mole^{-1} or less.

The standard molal entropies and volumes of H_2O at pressures above 10 kb and temperatures < 800°C represented by the smooth curves in figures 4, 5, and 6 were calculated from the partial derivatives of eq (15), which can be written as

$$S^\circ_{P,T,\hat{\imath}} = -\left(\frac{\partial \Delta G^\circ_{\hat{\imath}}}{\partial T}\right)_P = \sum_{j=1}^{4}\sum_{l=1}^{4-j} j a_{jl} T^{j-1} P^l \qquad (16)$$

and

$$V^\circ_{P,T,\hat{\imath}} = \left(\frac{\partial \Delta G^\circ_{\hat{\imath}}}{\partial P}\right)_T = \sum_{j=1}^{4}\sum_{l=1}^{4-j} l a_{jl} T^j P^{l-1} \qquad (17)$$

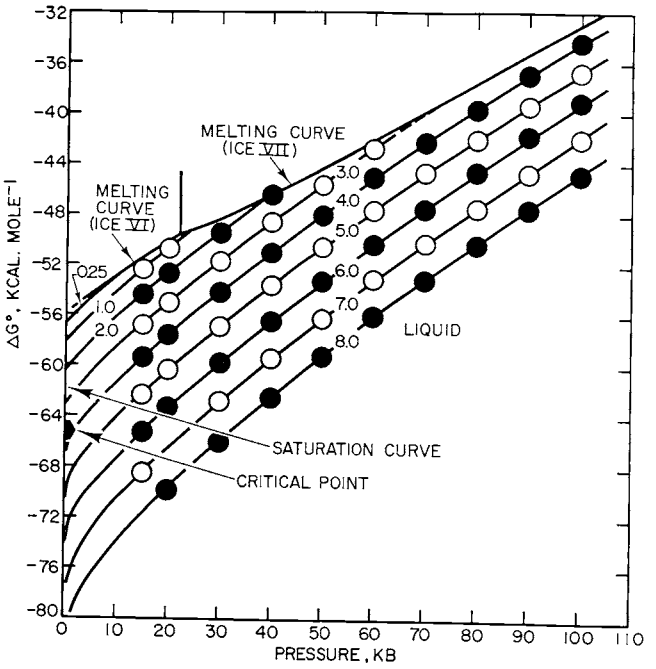

Fig. 3. Apparent standard molal Gibbs free energy of H_2O (table 2) as a function of pressure at constant temperature (labeled in °C × 10^{-2}) computed (curves) from eq (15) and the coefficients in table 1 for pressures > 10 kb — see caption for figure 2.

TABLE 2

Apparent standard molal Gibbs free energy of formation of H_2O in kcal $mole^{-1}$ computed from eq (15) and the coefficients in table 1 for pressures > 10 kb. The 10 kb values were calculated from equations given by Helgeson and Kirkham (1974).

T (°C)	PRESSURE, KB										
	10	15	20	30	40	50	60	70	80	90	100
25											
50	-53.28	-51.57									
75	-53.70	-51.98									
100	-54.16	-52.42	-50.76								
125	-54.64	-52.89	-51.21								
150	-55.15	-53.38	-51.69	-48.49							
175	-55.68	-53.90	-52.19	-48.98							
200	-56.23	-54.43	-52.72	-49.48	-46.43						
225	-56.80	-54.99	-53.27	-50.00	-46.94						
250	-57.39	-55.57	-53.83	-50.55	-47.47	-44.52					
275	-58.01	-56.17	-54.42	-51.11	-48.01	-45.05	-42.19				
300	-58.63	-56.79	-55.02	-51.69	-48.58	-45.60	-42.73	-39.94			
325	-59.28	-57.42	-55.64	-52.29	-49.16	-46.17	-43.29	-40.48	-37.75		
350	-59.94	-58.07	-56.27	-52.90	-49.75	-46.75	-43.86	-41.05	-38.31	-35.66	
375	-60.62	-58.73	-56.92	-53.53	-50.36	-47.35	-44.44	-41.62	-38.88	-36.22	-33.69
400	-61.31	-59.41	-57.59	-54.17	-50.99	-47.96	-45.04	-42.21	-39.46	-36.80	-34.26
425	-62.02	-60.10	-58.27	-54.83	-51.62	-48.58	-45.65	-42.82	-40.05	-37.38	-34.83
450	-62.74	-60.81	-58.96	-55.50	-52.27	-49.21	-46.28	-43.43	-40.66	-37.98	-35.42
475	-63.47	-61.53	-59.67	-56.18	-52.94	-49.87	-46.92	-44.06	-41.28	-38.59	-36.02
500	-64.21	-62.26	-60.38	-56.88	-53.61	-50.53	-47.56	-44.70	-41.91	-39.91	-36.63
525	-64.97	-63.00	-61.11	-57.58	-54.30	-51.20	-48.22	-45.35	-42.55	-39.84	-37.26
550	-65.74	-63.75	-61.85	-58.29	-54.99	-51.88	-48.89	-46.01	-43.20	-40.49	-37.89
575	-66.52	-64.52	-62.60	-59.02	-55.70	-52.57	-49.57	-46.68	-43.86	-41.14	-38.53
600	-67.31	-65.29	-63.36	-59.75	-56.42	-53.27	-50.27	-47.36	-44.54	-41.80	-39.18
625	-68.11	-66.07	-64.13	-60.50	-57.15	-53.99	-50.97	-48.05	-45.22	-42.48	-39.85
650	-68.93	-66.87	-64.91	-61.26	-57.88	-54.71	-51.68	-48.75	-45.91	-43.16	-40.52
675	-69.75	-67.67	-65.70	-62.02	-58.63	-55.44	-52.40	-49.46	-46.61	-43.85	-41.20
700	-70.58	-68.49	-66.50	-62.80	-59.39	-56.18	-53.13	-50.18	-47.32	-44.55	-41.89
725	-71.43	-69.31	-67.31	-63.59	-60.15	-56.94	-53.87	-50.91	-48.04	-45.27	-42.60
750	-72.28	-70.15	-68.13	-64.38	-60.93	-57.70	-54.62	-51.65	-48.88	-45.99	-43.31
775	-73.14	-70.99	-68.96	-65.19	-61.71	-58.47	-55.38	-52.40	-49.52	-46.72	-44.03
800	-74.01	-71.84	-69.80	-66.00	-62.51	-59.25	-56.15	-53.27	-50.27	-47.46	-44.77

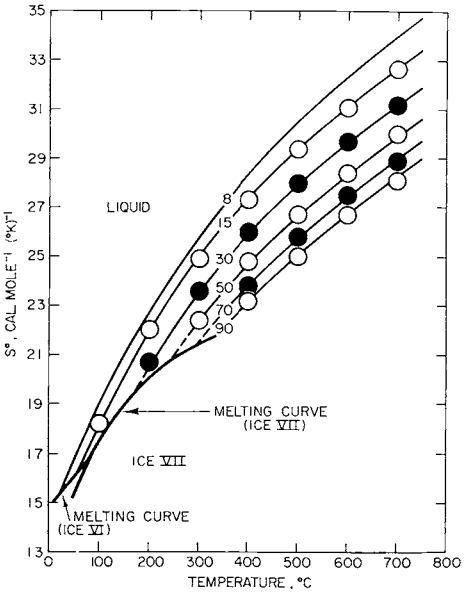

Fig. 4. Standard molal third law entropy of H_2O (table 3) as a function of temperature at constant pressure (labeled in kb) computed (curves) from eq (16) and the coefficients in table 1 for pressures > 10 kb. The curve for 8 kb was generated with the aid of equations given by Helgeson and Kirkham (1974) and the symbols represent values computed from those reported by Jüza (1966) — see text.

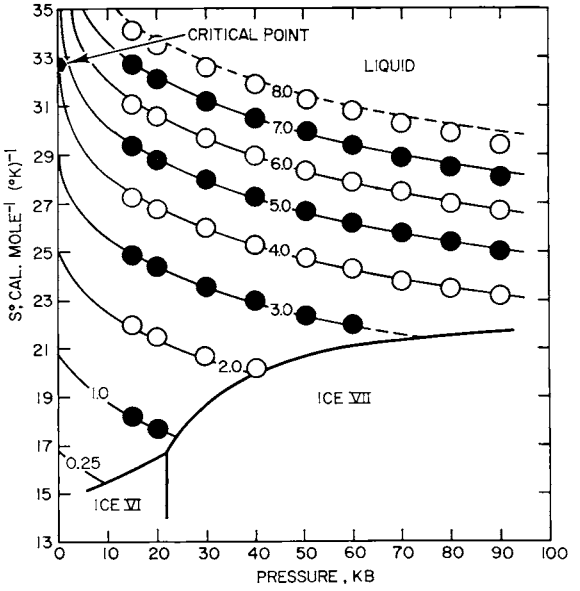

Fig. 5. Standard molal third law entropy of H_2O (table 3) as a function of pressure at constant temperature (labeled in °C × 10^{-3}) computed (curves) from eq (16) and the coefficients in table 1 for pressures > 10 kb — see caption for fig. 4.

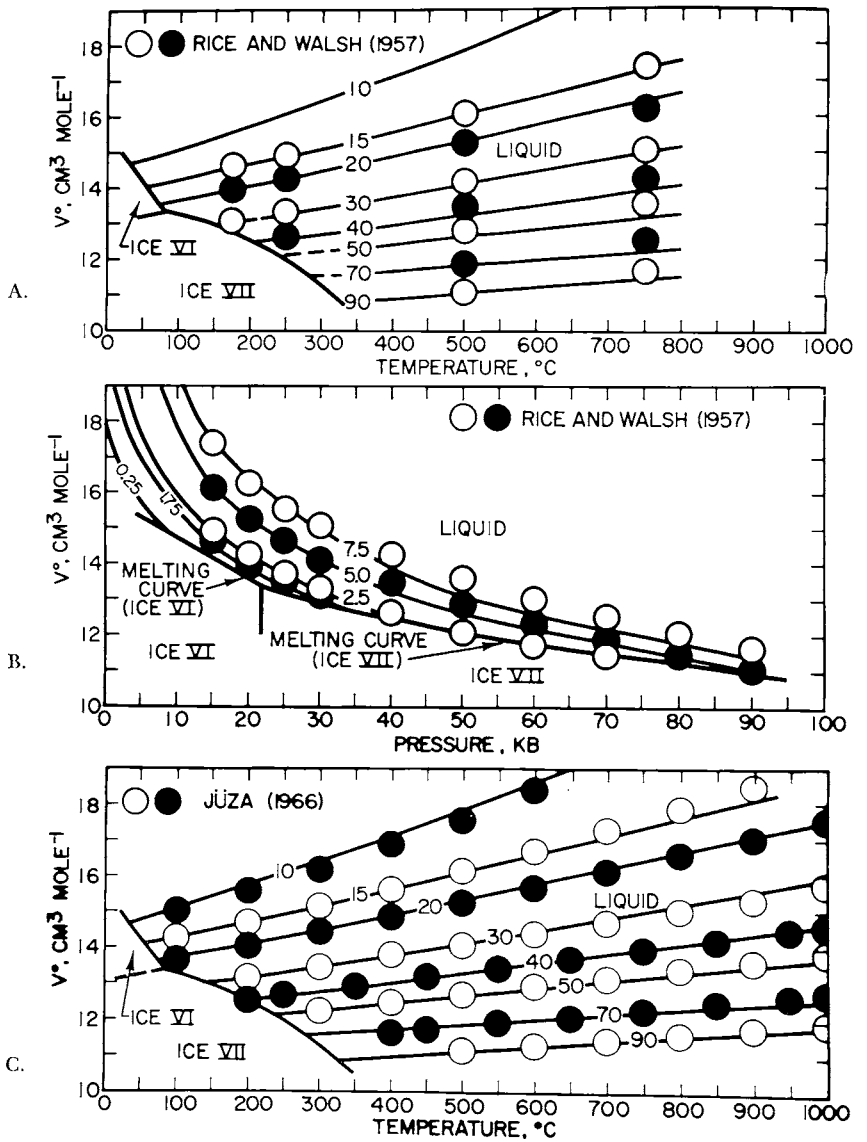

Fig. 6. Standard molal volume of H_2O (table 4) as a function of temperature at constant pressure (labeled in kb) and pressure at constant temperature (labeled in °C $\times 10^{-2}$) computed (curves) from eq (17) and the coefficients in table 1 for pressures > 10 kb. The curves for pressures at and below 10 kb were generated with the aid of equations given by Helgeson and Kirkham (1974). The symbols in figures 6A and B represent experimental values reported by Rice and Walsh (1957), but those in figure 6C were calculated from densities given by Jüza (1966) — see text.

The values of $S°_{P,T,\hat{i}}$ computed from eq (16) are in close agreement with corresponding values (represented by the symbols in figs. 4 and 5) calculated directly from entropies reported by Jüza (1966). The latter entropies, which are consistent with the convention, $S_{liquid\ H_2O} = 0$ at the triple point, were used together with

$$S°_{P,T,\hat{i}} = S°_{10^4,T,\hat{i}} + (S_{P,T,\hat{i}} - S_{10^4,T,\hat{i}}) \tag{18}$$

and values of $S°_{10^4,T,\hat{i}}$ (the standard molal third law entropy of H_2O at 10 kb and T) taken from Helgeson and Kirkham (1974) to calculate the standard molal entropies corresponding to the symbols in figures 4 and 5. It can be seen that the discrepancies between the curves and symbols in these figures are of the order of 0.5 cal mole^{-1} (°K)$^{-1}$ or less.

Comparison of standard molal volumes of H_2O computed from eq (17) for pressures > 10 kb with those calculated from shock-wave data by Rice and Walsh (1957) indicates that the two are in close agreement below ~ 500°C but depart slightly (up to ~ 0.5 cm^3 mole^{-1}) at 750°C above ~ 40 km (figs. 6A and B). The fact that Rice and Walsh assumed $(\partial H°/\partial V°)_P$ to be independent of temperature and $C°_P$ for H_2O to be constant at 25 kb in computing densities from their shock wave data probably accounts for the small discrepancies between the curves and

TABLE 3

Standard molal third law entropy of H_2O in cal mole^{-1} (°K)$^{-1}$ computed from eq (16) and the coefficients in table 1 for pressures > 10 kb. The 10 kb values were calculated from equations given by Helgeson and Kirkham (1974).

T	PRESSURE, KB										
(°C)	10	15	20	30	40	50	60	70	80	90	100
25											
50	16.45	15.98									
75	17.64	17.11									
100	18.73	18.18	17.70								
125	19.75	19.20	18.71								
150	20.71	20.16	19.67	18.85							
175	21.61	21.07	20.57	19.75							
200	22.46	21.94	21.44	20.59	19.95						
225	23.27	22.76	22.25	21.40	20.74						
250	24.05	23.54	23.02	22.16	21.49	20.98					
275	24.79	24.28	23.75	22.88	22.20	21.68	21.27				
300	25.49	24.98	24.45	23.56	22.88	22.34	21.93	21.59			
325	26.17	25.64	25.11	24.21	23.52	22.97	22.55	22.20	21.89		
350	26.81	26.27	25.73	24.83	24.12	23.57	23.14	22.78	22.47	22.14	
375	27.43	26.86	26.32	25.41	24.70	24.14	23.70	22.34	23.01	22.69	22.32
400	28.01	27.43	26.89	25.97	25.25	24.68	24.24	23.87	23.54	23.20	22.83
425	28.58	27.97	27.42	26.50	25.77	25.20	24.75	24.37	24.04	23.70	23.32
450	29.11	28.49	27.93	27.00	26.27	25.69	25.24	24.86	24.51	24.17	23.79
475	29.62	28.98	28.42	27.49	26.75	26.17	25.70	25.32	24.97	24.63	24.24
500	30.10	29.45	28.89	27.95	27.21	26.62	26.16	25.77	25.42	25.07	24.68
525	30.53	29.90	29.34	28.40	27.65	27.06	26.59	26.20	25.85	25.49	25.10
550	30.99	30.34	29.78	28.83	28.08	27.49	27.01	26.62	26.26	25.91	25.51
575	31.34	30.77	30.20	29.25	28.50	27.90	27.43	27.03	26.67	26.32	25.92
600	31.81	31.18	30.61	29.66	28.90	28.31	27.83	27.43	27.07	26.72	26.32
625	32.27	31.58	31.02	30.06	29.30	28.70	28.22	27.83	27.47	27.11	26.71
650	32.71	31.98	31.41	30.45	29.70	29.10	28.62	28.22	27.86	27.50	27.11
675	33.14	32.37	31.80	30.84	30.09	29.49	29.01	28.61	28.25	27.90	27.50
700	33.55	32.76	32.19	31.23	30.47	29.83	29.40	29.00	28.65	28.29	27.90
725	33.94	33.15	32.58	31.62	30.87	30.27	29.79	29.40	29.05	28.69	28.30
750	34.31	33.54	32.97	32.02	31.26	30.67	30.19	29.80	29.44	29.10	28.71
775	34.65	33.93	33.37	32.41	31.66	31.07	30.60	30.21	29.86	29.52	29.13
800	34.98	34.34	33.77	32.82	32.07	31.48	31.01	30.63	30.28	29.94	29.56

experimental data points in figures 6A and B at high pressures and temperatures. In contrast, it can be seen in figure 6C that the curves generated from eq (17) are in close agreement with densities computed by Jüza (1966), which are not dependent on these assumptions and differ somewhat from those calculated by Rice and Walsh.

Standard molal entropies and volumes of H_2O computed from eqs (16) and (17) are given in tables 3 and 4. Corresponding values of $\Delta H^\circ_{P,T,\hat{i}}$ and $\Delta A^\circ_{P,T,\hat{i}}$ (the apparent standard molal enthalpy and Helmholtz free energy of formation of H_2O) are shown in tables 5 and 6. The latter values were computed from

$$\Delta H^\circ_{P,T,\hat{i}} = \Delta H^\circ_{10^4,T,\hat{i}} + (\Delta G^\circ_{P,T,\hat{i}} - \Delta G^\circ_{10^4,T,\hat{i}}) + T(S^\circ_{P,T,\hat{i}} - S^\circ_{10^4,T,\hat{i}}) \tag{19}$$

and

$$\Delta A^\circ_{P,T,\hat{i}} = \Delta A^\circ_{10^4,T,\hat{i}} + (\Delta G^\circ_{P,T,\hat{i}} - \Delta G^\circ_{10^4,T,\hat{i}}) - PV^\circ_{P,T,\hat{i}} + 10^4 V^\circ_{10^4,T,\hat{i}} \tag{20}$$

using values of $\Delta G^\circ_{P,T,\hat{i}}$, $S^\circ_{P,T,\hat{i}}$, and $V^\circ_{P,T,\hat{i}}$ taken from tables 2 through 4 together with equations given by Helgeson and Kirkham (1974) to calculate $\Delta H^\circ_{10^4,T,\hat{i}}$ and $\Delta A^\circ_{10^4,T,\hat{i}}$ (the apparent standard molal enthalpy and Helmholtz free energy of formation of H_2O at 10 kb and T).

TABLE 4

Standard molal volume of H_2O in cm^3 $mole^{-1}$ computed from eq(17) and the coefficients in table 1 for pressures > 10 kb. The 10 kb values were calculated from equations given by Helgeson and Kirkham (1974).

T	PRESSURE, KB										
(°C)	10	15	20	30	40	50	60	70	80	90	100
25											
50	14.79	14.01									
75	14.96	14.12	13.57								
100	15.11	14.22	13.67								
125	15.27	14.33	13.76								
150	15.42	14.44	13.86	12.96							
175	15.58	14.55	13.96	13.04							
200	15.74	14.66	14.05	13.11	12.46						
225	15.90	14.77	14.15	13.19	12.52						
250	16.07	14.89	14.26	13.27	12.58	12.11					
275	16.25	15.00	14.36	13.35	12.64	12.16	11.81				
300	16.42	15.12	14.46	13.43	12.70	12.20	11.84	11.54			
325	16.60	15.24	14.57	13.51	12.77	12.25	11.88	11.58	11.25		
350	16.77	15.36	14.67	13.59	12.83	12.30	11.92	11.61	11.28	10.85	
375	16.95	15.47	14.78	13.68	12.90	12.35	11.97	11.65	11.31	10.88	10.31
400	17.13	15.59	14.89	13.76	12.96	12.41	12.01	11.68	11.35	10.92	10.35
425	17.31	15.72	14.99	13.85	13.03	12.46	12.05	11.72	11.38	10.95	10.40
450	17.50	15.84	15.10	13.93	13.10	12.51	12.09	11.75	11.42	10.99	10.44
475	17.68	15.96	15.21	14.02	13.17	12.57	12.14	11.79	11.45	11.03	10.49
500	17.86	16.08	15.32	14.11	13.23	12.62	12.18	11.83	11.49	11.07	10.53
525	18.06	16.21	15.43	14.20	13.30	12.67	12.22	11.87	11.52	11.10	10.58
550	18.24	16.33	15.54	14.28	13.37	12.73	12.27	11.91	11.56	11.14	10.62
575	18.44	16.45	15.65	14.37	13.44	12.78	12.31	11.94	11.60	11.18	10.67
600	18.63	16.58	15.77	14.46	13.51	12.84	12.36	11.98	11.63	11.22	10.71
625	18.84	16.70	15.88	14.55	13.58	12.90	12.40	12.02	11.67	11.26	10.76
650	19.04	16.83	15.99	14.64	13.65	12.95	12.45	12.06	11.71	11.30	10.80
675	19.25	16.95	16.10	14.73	13.72	13.01	12.49	12.10	11.74	11.34	10.85
700	19.47	17.08	16.21	14.82	13.79	13.06	12.54	12.14	11.78	11.38	10.89
725	19.69	17.20	16.33	14.91	13.86	13.12	12.58	12.18	11.81	11.41	10.93
750	19.91	17.33	16.44	14.99	13.93	13.17	12.63	12.22	11.85	11.45	10.98
775	20.13	17.45	16.55	15.08	14.00	13.23	12.67	12.25	11.89	11.49	11.02
800	20.35	17.58	16.66	15.17	14.07	13.28	12.72	12.29	11.92	11.53	11.06

Log fugacities of H_2O consistent with the standard state conventions adopted by Helgeson and Kirkham (1974) are given in table 7 for pressures $\geqslant$ 10 kb and temperatures $\leqslant$ 800°C. The fugacities were computed from

$$\log f_{P,T,\hat{i}} = \frac{1}{2.303RT}\left(G^\circ_{P,T,\hat{i}} - G^\circ_{10^1,T,\hat{i}}\right) + \log f_{10^1,T,\hat{i}} \qquad (21)$$

using the apparent standard molal Gibbs free energies of formation of H_2O in table 2 together with values of $f_{10^1,T,\hat{i}}$ calculated from equations given by Helgeson and Kirkham (1974).

It can be seen in table 7 that increasing pressure from 10 to 100 kb causes an increase in the fugacity of H_2O of up to seven orders of magnitude. Such large positive departures from ideality strongly promote accelerated reaction rates at high pressures (Ahrens and Schubert, 1975). Under conditions of $P_{H_2O} << P_{fluid}$ and/or low water to rock ratios, H_2O (or more precisely, the hydronium ion) is apparently effective in breaking silicon-oxygen bonds, which facilitates interstitial cation diffusion in silicates and breakdown of metastable phases (Burte and Nicholson, 1972; Ahrens and Schubert, 1975).

Thermodynamics of dehydration reactions.—The law of mass action for reaction (3) can be written as

$$\prod_{i=1}^{\hat{i}} a_i^{\tilde{n}_i} = K \qquad (22)$$

where a_i and $\tilde{n}_i$ refer to the activity and reaction coefficient of the ith mineral component, respectively, and K stands for the equilibrium constant for the reaction, which is defined by

$$K \equiv e^{-\Delta G^\circ_{P,T,r}/RT} \qquad (23)$$

where $\Delta G^\circ_{P,T,r}$ denotes the standard molal Gibbs free energy of reaction. Recalling that $\hat{i}$ designates H_2O, we can write for $i = 1, 2, \ldots (\hat{i}-1)$

$$a_i = \lambda_i X_i \qquad (24)$$

where λ_i and X_i correspond to the activity coefficient and mole fraction of the subscripted species. Accordingly, eq (22) can be expressed as

$$a_{\hat{i}}^{\tilde{n}_{\hat{i}}} \prod_{i=1}^{\hat{i}-1} \lambda_i^{\tilde{n}_i} X_i^{\tilde{n}_i} = K \qquad (25)$$

For reactions among stoichiometric minerals, eq (25) reduces to

$$a_{\hat{i}}^{\tilde{n}_{\hat{i}}} = K \qquad (26)$$

Solubility studies (for example, Morey and Hesselgesser, 1951; Morey, 1957; Hemley, 1959; Hemley, Meyer, and Richter, 1961; Hemley and

TABLE 5

Apparent standard molal enthalpy of formation of H_2O in kcal mole^{-1} computed from eq (19) using apparent standard molal Gibbs free energies of formation and standard molal third law entropies of H_2O taken from tables 2 and 3 together with values of $\Delta H^\circ_{10^4,T,\hat{l}}$ generated from equations given by Helgeson and Kirkham (1974).

T	PRESSURE, KB										
(°C)	10	15	20	30	40	50	60	70	80	90	100
25											
50	-64.57	-63.01									
75	-64.18	-62.63									
100	-63.78	-62.25	-60.76								
125	-63.39	-61.85	-60.37								
150	-63.00	-61.46	-59.98	-57.12							
175	-62.61	-61.06	-59.58	-56.73							
200	-62.22	-60.66	-59.19	-56.34	-53.60						
225	-61.82	-60.26	-58.79	-55.96	-53.21						
250	-61.43	-59.87	-58.40	-55.57	-52.83	-50.15					
275	-61.03	-59.47	-58.00	-55.18	-52.45	-49.78	-47.14				
300	-60.64	-59.08	-57.62	-54.80	-52.07	-49.40	-46.77	-44.17			
325	-60.24	-58.69	-57.23	-54.42	-51.70	-49.04	-46.41	-43.81	-41.27		
350	-59.85	-58.31	-56.85	-54.04	-51.33	-48.67	-46.05	-43.46	-40.92	-38.47	
375	-59.45	-57.93	-56.47	-53.67	-50.96	-48.31	-45.69	-43.10	-40.57	-38.13	-35.84
400	-59.07	-57.55	-56.10	-53.30	-50.60	-47.95	-45.34	-42.75	-40.23	-37.79	-35.50
425	-58.68	-57.18	-55.73	-52.94	-50.24	-47.60	-44.99	-42.41	-39.88	-37.45	-35.16
450	-58.30	-56.82	-55.37	-52.58	-49.89	-47.25	-44.64	-42.07	-39.54	-37.11	-34.83
475	-57.92	-56.46	-55.01	-52.22	-49.53	-26.90	-44.29	-41.72	-39.20	-36.78	-34.50
500	-57.55	-56.10	-54.65	-51.87	-49.18	-46.55	-43.95	-41.38	-38.87	-36.44	-34.16
525	-57.22	-55.74	-54.30	-51.52	-48.84	-46.21	-43.61	-41.04	-38.53	-36.11	-33.83
550	-56.84	-55.39	-53.94	-51.17	-48.49	-45.86	-43.27	-40.70	-38.19	-35.77	-33.50
575	-56.55	-55.03	-53.59	-50.82	-48.14	-45.52	-42.92	-40.36	-37.85	-35.43	-33.16
600	-56.15	-54.68	-53.24	-50.47	-47.79	-45.17	-42.58	-40.02	-37.51	-35.08	-32.81
625	-55.74	-54.32	-52.88	-50.11	-47.44	-44.82	-42.22	-39.66	-37.16	-34.73	-32.46
650	-55.34	-53.96	-52.52	-49.75	-47.08	-44.46	-41.87	-39.31	-36.80	-34.38	-32.10
675	-54.94	-53.59	-52.16	-49.39	-46.71	-44.09	-41.50	-38.94	-36.43	-34.01	-31.73
700	-54.55	-53.22	-51.78	-49.01	-46.34	-43.72	-41.13	-38.56	-36.05	-33.63	-31.35
725	-54.16	-53.83	-51.40	-48.63	-45.95	-43.33	-40.74	-38.17	-35.66	-33.23	-30.96
750	-53.79	-52.44	-51.00	-48.23	-45.56	-42.93	-40.33	-37.77	-35.25	-32.82	-30.54
775	-53.44	-52.03	-50.59	-47.82	-45.14	-42.51	-39.91	-37.35	-34.83	-32.39	-30.11
800	-53.09	-51.60	-50.16	-47.39	-44.70	-42.08	-39.47	-36.90	-34.38	-31.94	-29.65

TABLE 6

Apparent standard molal Helmholtz free energy of formation of H_2O in kcal mole^{-1} computed from eq (20) using apparent standard molal Gibbs free energies of formation and standard molal volumes of H_2O taken from tables 2 and 4 together with values of $\Delta A^\circ_{10^4,T,\hat{l}}$ generated from equations given by Helgeson and Kirkham (1974).

T	PRESSURE, KB										
(C°)	10	15	20	30	40	50	60	70	80	90	100
25											
50	-55.94	-55.71									
75	-56.40	-56.16									
100	-56.90	-56.64	-56.41								
125	-57.42	-57.15	-56.91								
150	-57.96	-57.68	-57.44	-56.91							
175	-58.53	-58.23	-57.99	-57.44							
200	-59.12	-58.81	-58.56	-58.00	-57.46						
225	-59.73	-59.41	-59.15	-58.58	-58.03						
250	-60.36	-60.03	-59.77	-59.19	-58.61	-58.61					
275	-61.01	-60.67	-60.40	-59.81	-59.22	-59.22	-58.24				
300	-61.68	-61.33	-61.05	-60.44	-59.84	-59.84	-58.84	-58.37			
325	-62.37	-62.00	-61.72	-61.10	-60.48	-60.48	-59.45	-58.97	-58.38		
350	-63.08	-62.69	-62.41	-61.77	-61.14	-61.14	-60.08	-59.59	-59.00	-58.11	
375	-63.79	-63.40	-63.11	-62.46	-61.81	-61.81	-60.72	-60.23	-59.63	-58.75	-57.36
400	-64.53	-64.12	-63.83	-63.16	-62.50	-62.50	-61.38	-60.88	-60.28	-59.40	-58.02
425	-65.28	-64.86	-64.56	-63.88	-63.20	-63.20	-62.05	-61.54	-60.94	-60.07	-58.70
450	-66.04	-65.61	-65.30	-64.61	-63.92	-63.92	-62.74	-62.22	-61.61	-60.75	-59.40
475	-66.82	-66.37	-66.06	-65.36	-64.65	-64.65	-63.44	-62.91	-62.30	-61.44	-60.10
500	-67.61	-67.15	-66.83	-66.11	-65.39	-65.39	-64.15	-63.61	-62.99	-62.14	-60.82
525	-68.41	-67.93	-67.61	-66.88	-66.14	-66.14	-64.88	-64.32	-63.70	-62.85	-61.55
550	-69.22	-68.73	-68.40	-67.66	-66.90	-66.90	-65.61	-65.05	-64.43	-63.58	-62.29
575	-70.05	-69.54	-69.20	-68.45	-67.68	-67.68	-66.35	-65.78	-65.16	-64.32	-63.04
600	-70.89	-70.36	-70.02	-69.25	-68.46	-68.46	-67.11	-66.53	-65.90	-65.06	-63.80
625	-71.74	-71.19	-70.84	-70.06	-69.25	-69.25	-67.88	-67.28	-66.65	-65.82	-64.57
650	-72.61	-72.03	-71.68	-70.88	-70.06	-70.06	-68.65	-68.05	-67.41	-66.58	-65.35
675	-73.48	-72.87	-72.52	-71.71	-70.87	-70.87	-69.43	-68.83	-68.18	-67.36	-66.14
700	-74.36	-73.73	-72.37	-72.55	-71.70	-71.70	-70.23	-69.61	-68.97	-68.15	-66.94
725	-75.26	-74.60	-74.24	-73.40	-72.53	-72.53	-71.03	-70.40	-69.76	-68.94	-67.75
750	-76.16	-75.48	-75.11	-74.25	-73.37	-73.37	-71.85	-71.21	-70.56	-69.74	-68.57
775	-77.08	-76.37	-75.99	-75.12	-74.23	-74.23	-72.67	-72.02	-71.37	-70.56	-69,39
800	-78.00	-77.27	-76.88	-76.00	-75.09	-75.09	-73.51	-72.85	-72.19	-71.38	-70.23

others, 1971, 1977a, b; Orville, 1963, 1972; Weill and Fyfe, 1964; Anderson and Burnham, 1965) and fluid inclusion analyses (Roedder, 1972; Touret, 1971a, b, 1974; Poty and Stalder, 1970; Poty, Stalder, and Weisbrod, 1974) suggest that aqueous solutions involved in metamorphic processes at high temperatures and pressures contain up to a few percent dissolved solids in addition to CO_2, methane, and other gases. Although it has been suggested that CO_2 is the dominant volatile in the mantle (Roedder, 1965; Green and Radcliffe, 1975; Green, 1972; Anderson, 1975; Eggler, 1976; Mysen and others, 1976; Wyllie and Huang, 1976) the relative extent to which CO_2 and H_2O are present in the fluid released by dehydration/decarbonation reactions in subducting lithosphere has yet to be demonstrated. However, recent analyses seem to indicate that H_2O is the most abundant component of fluid inclusions in diamonds (Melton and Giardini, 1975), which also contain solid inclusions of biotite (Giardini and others, 1974).

The high-temperature limiting case for stoichiometric minerals in equilibrium with an H_2O-rich fluid can be examined in terms of the standard state adopted above by setting $a_i = 1$ in eq (26) so that

$$K = 1 \tag{27}$$

TABLE 7

Log fugacity of H_2O computed from eq (21) using apparent standard molal Gibbs free energies of formation of H_2O taken from table 2 together with values of log $f_{10^3,T,\hat{i}}$ generated from equations given by Helgeson and Kirkham (1974).

T	PRESSURE, KB										
(°C)	10	15	20	30	40	50	60	70	80	90	100
25											
50	1.704	2.860									
75	2.304	3.113									
100	2.311	3.330	4.302								
125	2.547	3.508	4.430								
150	2.750	3.664	4.537	6.190							
175	2.926	3.794	4.628	6.193							
200	3.078	3.909	4.699	6.195	7.604						
225	3.211	4.005	4.759	6.194	7.536						
250	3.327	4.087	4.814	6.184	7.471	8.703					
275	3.430	4.163	4.861	6.180	7.416	8.596	9.736				
300	3.520	4.221	4.896	6.166	7.351	8.487	9.581	10.645			
325	3.600	4.279	4.929	6.153	7.297	8.389	9.441	10.467	11.465		
350	3.671	4.327	4.958	6.139	7.244	8.296	9.309	10.295	11.255	12.185	
375	3.734	4.371	4.982	6.125	7.193	8.208	9.189	10.140	10.063	11.960	12.813
400	3.791	4.408	4.999	6.109	7.141	8.125	9.072	9.991	10.884	11.747	12.572
425	3.842	4.443	5.016	6.092	7.097	8.048	8.965	9.851	10.718	11.554	12.352
450	3.888	4.471	5.030	6.075	7.051	7.976	8.861	9.722	10.559	11.369	12.143
475	3.929	4.495	5.038	6.058	7.004	7.901	8.762	9.598	10.410	11.195	11.946
500	3.966	4.517	5.048	6.037	6.962	7.832	8.671	9.480	10.268	10.833	11.760
525	3.999	4.539	5.056	6.022	6.920	7.769	8.585	9.371	10.137	10.879	11.585
550	4.030	4.558	5.062	6.077	6.883	7.709	8.502	9.267	10.013	10.732	11.422
575	4.057	4.572	5.067	5.990	6.844	7.651	8.424	9.168	9.895	10.595	11.268
600	4.081	4.587	5.070	5.973	6.807	7.595	8.346	9.074	9.780	10.465	11.121
625	4.104	4.600	5.072	5.955	6.770	7.539	8.273	8.984	9.672	10.339	10.979
650	4.124	4.611	5.075	5.939	6.739	7.489	8.207	8.900	9.572	10.223	10.848
675	4.142	4.621	5.075	5.923	6.704	7.439	8.140	8.818	9.474	10.110	10.721
700	4.158	4.627	5.074	5.905	6.671	7.391	8.076	8.739	9.381	10.003	10.600
725	4.173	4.637	5.075	5.889	6.642	7.345	8.017	8.665	9.293	9.900	10.484
750	4.186	4.641	5.073	5.873	6.610	7.300	7.958	8.592	9.184	9.801	10.373
775	4.198	4.647	5.070	5.856	6.581	7.257	7.901	8.552	9.123	9.706	10.267
800	4.210	4.651	5.067	5.840	6.551	7.215	7.846	8.432	9.043	9.615	10.163

at equilibrium, regardless of the pressure and temperature. Under these conditions, the equilibrium temperature at a given pressue is maximal and corresponds to the temperature at which $\Delta G^\circ_r = 0$, where

$$\Delta H^\circ_r = T\Delta S^\circ_r \tag{28}$$

and

$$\left(\frac{\partial P}{\partial T}\right)_{\Delta G^\circ_r = 0} = \frac{\Delta S^\circ_r}{\Delta V^\circ_r} = \frac{\Delta H^\circ_r}{T\Delta V^\circ_r} \tag{29}$$

If CO_2 is present in the fluid phase in significant concentrations and/or minerals involved in the dehydration process exhibit appreciable solid solution, $K \neq 1$ and the equilibrium temperature at a given pressure corresponds to the temperature at which eq (25) is satisfied.

CALCULATION OF PHASE RELATIONS AT HIGH PRESSURES AND TEMPERATURES

The equations summarized above can be combined with thermodynamic data for minerals at 25°C and 1 bar to describe quantitatively phase relations in rocks at pressures and temperatures corresponding to those in the upper mantle. Calculations of this kind make it possible to fill in gaps left by experimental investigations of phase equilibria and permit extension of univariant curves to pressures and temperatures beyond experimental capabilities. Because the thermodynamic data for minerals summarized recently by Helgeson, Delany, Nesbitt, and Bird (1978) are internally consistent, comprehensive, and compatible with both geologic observations and experimental data at low pressures, they afford a reasonable basis for extrapolation of equilibrium calculations to high pressures and temperatures. These data were used together with the equations derived in the preceding pages and those given by Helgeson and Kirkham (1974) to generate univariant dehydration curves at high pressures for a large number of reactions among minerals in subducting oceanic crust.

Because the expansibility and compressibility of α-quartz are anomalously high compared to other minerals (Birch, 1966; Skinner, 1966), the algorithm suggested by Helgeson, Delany, Nesbitt, and Bird (1978) was used in the calculations to represent V°_i for α-quartz as a function of pressure and temperature. The thermal expansion and compressibility of α-quartz have a significant effect on computed equilibrium temperatures and pressures for a number of solid/solid reactions in the system Al_2O_3–SiO_2–H_2O (see below). The α/β quartz transition was treated in the calculations as a pseudo-first-order transition (Helgeson, Delany, Nesbitt, and Bird, 1978).

Many univariant equilibrium curves are terminated at high pressures by invariant points that have not yet been defined experimentally. As a consequence, a number of the calculations and extrapolations reported by Anderson, Uyeda, and Miyashiro (1976) are misleading. In calculating the thermodynamic properties of dehydration reactions, Anderson, Uyeda, and Miyashiro took no account of invariant equilibria, and their extrapolations to high pressures were uncontrolled. To

insure geologic relevance of univariant equilibrium calculations, all invariant points in a given system must be located and metastable phase assemblages identified. Schreinemaker's rules (Schreinemaker, 1916; Zen, 1966) facilitate such distinctions.

The systems $MgO–SiO_2–H_2O$ and $Al_2O_3–SiO_2–H_2O$ are perhaps the most relevant to investigation of dehydration in subducting lithosphere. Minerals in these systems comprise much of the basalt, gabbro, greenschist, and amphibolite of the oceanic crust, as well as the sediment cover found on the ocean floor. Although experimental evidence suggests that hornblende, phlogopite, and other "complex" silicates play an important role in mantle processes (for example, see Kushiro, Syono, and Akimoto, 1967) the relative stabilities of these minerals depend to a large extent on

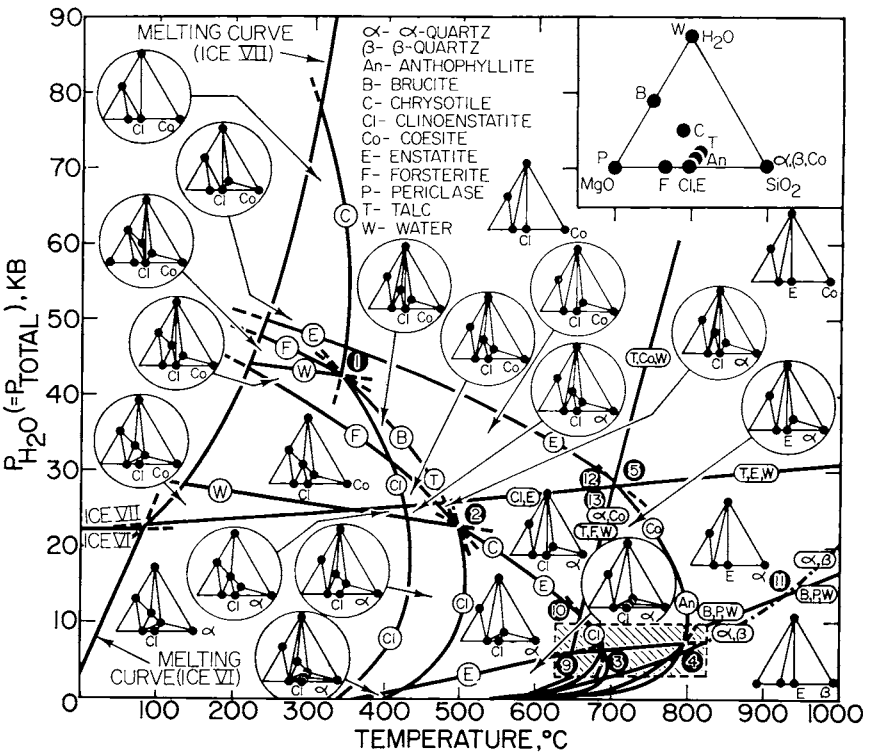

Fig. 7. Equilibrium phase relations in the system $MgO–SiO_2–H_2O$ generated without provision for antigorite (see text) from equations summarized above and those given by Helgeson and Kirkham (1974) using thermodynamic data for minerals taken from Helgeson, Delaney, Nesbitt, and Bird (1978). The configurations of the univariant curves and metastable extensions about invariant points (designated by circled numbers) are consistent with Schreinemaker's rules. The curves representing stable phase assemblages are labeled with circled letters indicating the absent phase (or phases) relative to each invariant assemblage. Melting curves other than those for ice VI and VII were omitted for the sake of clarity. Dashed lines indicate metastable extensions, but the dash-dot curves for the dehydration of brucite is an extrapolation (see text). The shaded portion of the figure is enlarged in figure 9.

the thermodynamic behavior of minerals in the systems $MgO–SiO_2–H_2O$ and $Al_2O_3–SiO_2–H_2O$.

The system $MgO–SiO_2–H_2O$.—Phase relations in this system at pressures and temperatures to 90 kb and > 800°C are depicted in figures 7 through 9. The univariant curves and invariant points shown in the first of these figures were generated by including provision for the occurrence of metastable chrysotile and its coexistence with talc, which is permitted only in the absence of stoichiometric antigorite (see below). The phase relations shown in figure 8 represent stable equilibrium in the system $MgO–SiO_2–H_2O$, and those depicted in figure 9 refer to the shaded regions in figures 7 and 8. The reactions corresponding to the curves in figures 7 through 9 are summarized in table 8. Mineral formulas for the phases are also shown in table 8, and the thermodynamic properties of many of the reactions at various pressures and temperatures are given in table 9. No provision was included in the calculations for minerals in the humite group or the dense hydrated magnesian silicates identified and characterized by Sclar, Carrison, and Schwartz (1965), Sclar and

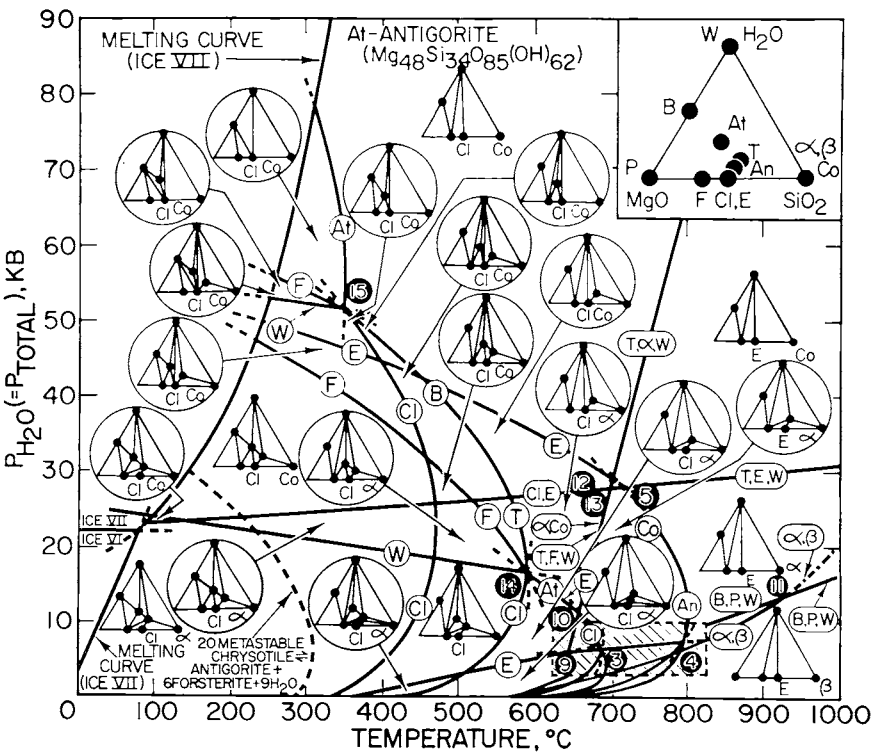

Fig. 8. Equilibrium phase relations in the system $MgO–SiO_2–H_2O$ generated from equations summarized above and those given by Helgeson and Kirkham (1974) using thermodynamic data for minerals taken from Helgeson, Delaney, Nesbitt, and Bird (1978) — see caption for figure 7.

TABLE 8

Summary of reactions in the systems $MgO–SiO_2–H_2O$ and $Al_2O_3–SiO_2–H_2O$ represented by univariant curves in figures 7 through 13, 16, 17, 19, 22, and 23 and the formulas of the minerals considered in the present study. The invariant point numbers (IP) and the letters designating the curves correspond to those shown in the figures.

IP	Curve	Mineral Reactions in the System $MgO-SiO_2-H_2O$
1	C	Brucite + Clinoenstatite $\rightleftharpoons$ Forsterite + H_2O
	B	Chrysotile $\rightleftharpoons$ Forsterite + Clinoenstatite + 2 H_2O
	Cℓ	Chrysotile + Brucite $\rightleftharpoons$ 2 Forsterite + 3 H_2O
	W	2 Brucite + 3 Clinoenstatite $\rightleftharpoons$ Forsterite + Chrysotile
	F	Chrysotile $\rightleftharpoons$ Brucite + 2 Clinoenstatite + H_2O
2	C	Talc + Forsterite $\rightleftharpoons$ 5 Clinoenstatite + H_2O
	Cℓ	5 Chrysotile $\rightleftharpoons$ Talc + 6 Forsterite + 9 H_2O
	W	Chrysotile + 9 Clinoenstatite $\rightleftharpoons$ 2 Talc + 3 Forsterite
	F	Chrysotile + Talc $\rightleftharpoons$ 6 Clinoenstatite + 3 H_2O
	T	Same as 1B
3	T	Anthophyllite + Forsterite $\rightleftharpoons$ 9 Enstatite + H_2O
	E	9 Talc + 4 Forsterite $\rightleftharpoons$ 5 Anthophyllite + 4 H_2O
	F,W	Talc + 4 Enstatite $\rightleftharpoons$ Anthophyllite
	An	Talc + Forsterite $\rightleftharpoons$ 5 Enstatite + H_2O
4	T	Anthophyllite $\rightleftharpoons$ 7 Enstatite + β-Quartz + H_2O
	E	7 Talc $\rightleftharpoons$ 3 Anthophyllite + 4 β-Quartz + 4 H_2O
	β,W	Same as 3F,W
	An	Talc $\rightleftharpoons$ 3 Enstatite + β-Quartz + H_2O
5	Co	Talc $\rightleftharpoons$ 3 Enstatite + α-Quartz + H_2O
	α	Talc $\rightleftharpoons$ 3 Enstatite + Coesite + H_2O
	T,E,W	α-Quartz $\rightleftharpoons$ Coesite
6	α,β	Same as 3F,W
	An,T,E	α-Quartz $\rightleftharpoons$ β-Quartz
7	α	Same as 4An
	β	Same as 5Co
	T,E,W	Same as 6An,T,E
8	Cℓ,E	Same as 6An,T,E
	α,β	Clinoenstatite $\rightleftharpoons$ Enstatite.

IP	Curve	Mineral Reactions in the System $Al_2O_3-SiO_2-H_2O$
1	G,W	Pyrophyllite $\rightleftharpoons$ 2 Diaspore + 4 α-Quartz
	[illegible],P	Gibbsite $\rightleftharpoons$ Diaspore + H_2O
	D	2 Gibbsite + 4α-Quartz $\rightleftharpoons$ Pyrophyllite + H_2O
2	[illegible],W	2 Kaolinite $\rightleftharpoons$ Pyrophyllite + 2 Gibbsite
	P	2 Gibbsite + 2 α-Quartz $\rightleftharpoons$ Kaolinite + H_2O
	Ka	Same as 1D
	G	Kaolinite + 2 α-Quartz $\rightleftharpoons$ Pyrophyllite + H_2O
3	P,Ka	Same as 1α,P
	G	2 Kaolinite $\rightleftharpoons$ Pyrophyllite + 2 Diaspore + 2 H_2O
	D,W	Same as 2W
4	K,W	Pyrophyllite $\rightleftharpoons$ 2 Diaspore + 4 Coesite + H_2O
	D	Pyrophyllite $\rightleftharpoons$ Kyanite + 3 Coesite + H_2O
	Co	Pyrophyllite + 6 Diaspore $\rightleftharpoons$ 4 Kyanite + 4 H_2O
	P	2 Diaspore + Coesite $\rightleftharpoons$ Kyanite + H_2O
5	α	Same as 4D
	K,P,W	α-Quartz $\rightleftharpoons$ Coesite
	Co	Pyrophyllite $\rightleftharpoons$ Kyanite + 3 α-Quartz + H_2O
6	K	Same as 3G
	Ka	Same as 4Co
	W	3 Pyrophyllite + 10 Diaspore $\rightleftharpoons$ 4 Kyanite + 4 Kaolinite
	P	Kaolinite + 2 Diaspore $\rightleftharpoons$ 2 Kyanite + 3 H_2O
	D	3 Kaolinite $\rightleftharpoons$ 2 Kyanite + Pyrophyllite + 5 H_2O
7	K	3 Pyrophyllite + 10 Diaspore $\rightleftharpoons$ 4 Andalusite + 4 Kaolinite
	Ka,D,P	Kyanite $\rightleftharpoons$ Andalusite
	A	Same as 6W
8	K	Kaolinite + 2 Diaspore $\rightleftharpoons$ 4 Andalusite + 3 H_2O
	A	Same as 6P
	Ka,D,W	Same as 7Ka,D,P

IP	Curve	Mineral Reactions in the System $MgO-SiO_2-H_2O$
9	An,T	Same as 8α,β
	E	Talc + 4 Clinoenstatite ⇄ Anthophyllite
	Cℓ	Same as 3F,W
10	E	Same as 2Cℓ
	Cℓ	Talc + Forsterite ⇄ 5 Enstatite + H_2O
	T,F,W	Same as 8α,β
11	B,P,W	Same as 6An,T,E
	α,β	Brucite ⇄ Periclase + H_2O
12	E	Talc ⇄ 3 Clinoenstatite + Coesite + H_2O
	Cℓ	Same as 5α
	T,Co,W	Same as 8α,β
13	α,Co	Same as 8α,β
	Cℓ,E	Same as 5T,E,W
14	At	Same as 2C
	F	Antigorite + 14 Talc ⇄ 90 Clinoenstatite + 45 H_2O
	T	Antigorite ⇄ 14 Forsterite + 20 Clinoenstatite + 31 H_2O
	Cℓ	Antigorite ⇄ 4 Talc + 18 Forsterite + 27 H_2O
	W	Antigorite + 135 Clinoenstatite ⇄ 31 Talc + 45 Forsterite
15	At	Same as 1Cℓ
	F	Antigorite ⇄ 14 Brucite + 34 Clinoenstatite + 17 H_2O
	W	31 Brucite + 51 Clinoenstatite ⇄ 17 Forsterite + Antigorite
	B	Same as 14T
	Cℓ	Antigorite + 20 Brucite ⇄ 34 Forsterite + 51 H_2O

Mineral	Formula	Mineral	Formula
Albite	$NaAlSi_3O_8$	Brucite	$Mg(OH)_2$
Andalusite	Al_2SiO_5	Chrysotile	$Mg_3Si_2O_5(OH)_4$
Annite	$KFe_3(AlSi_3O_{10})(OH)_2$	Clinochlore	$Mg_5Al(AlSi_3O_{10})(OH)_8$
Anorthite	$CaAl_2Si_2O_8$	Coesite	SiO_2
Anthophyllite	$Mg_7Si_8O_{22}(OH)_2$	Corundum	Al_2O_3
Antigorite	$Mg_{48}Si_{34}O_{85}(OH)_{62}$	Diaspore	$AlO(OH)$

IP	Curve	Mineral Reactions in the System $Al_2O_3-SiO_2-H_2O$
9	A	Same as 6D
	K	3 Kaolinite ⇄ 2 Andalusite + Pyrophyllite + 5 H_2O
	Ka,P,W	Same as 7Ka,D,P
10	A,K	2 Diaspore ⇄ Corundum + H_2O
	D,C,W	Same as 7Ka,D,P
11	A	Same as 5Co
	K	Pyrophyllite ⇄ Andalusite + 3 α-Quartz + H_2O
	P,α,W	Same as 7Ka,D,P
12	A	Kyanite ⇄ Sillimanite
	K	Andalusite ⇄ Sillimanite
	S	Same as 7Ka,D,P
13	α,Co	Same as 1α,P
	G,D,W	Same as 5K,P,W
14	Co	Same as 1G,W
	α	Same as 4K,W
	D,P,W	Same as 5K,P,W

Mineral	Formula	Mineral	Formula
Diopside	$CaMg(SiO_3)_2$	Periclase	MgO
Enstatite	$MgSiO_3$	Phlogopite	$KMg_3(AlSi_3O_{10})(OH)_2$
Ferrosilite	$FeSiO_3$	Prehnite	$Ca_2Al(AlSi_3O_{10})(OH)_2$
Forsterite	Mg_2SiO_4	Pyrophyllite	$Al_2Si_4O_{10}(OH)_2$
Gibbsite	$Al(OH)_3$	Quartz	SiO_2
Grossular	$Ca_3Al_2Si_3O_{12}$	Sillimanite	Al_2SiO_5
Jadeite	$NaAlSi_2O_6$	Spinel	$MgAl_2O_4$
Kaolinite	$Al_2Si_2O_5(OH)_4$	Talc	$Mg_3Si_4O_{10}(OH)_2$
K-feldspar	$KAlSi_3O_8$	Tremolite	$Ca_2Mg_5Si_8O_{22}(OH)_2$
Kyanite	Al_2SiO_5	Wollastonite	$CaSiO_3$
Muscovite	$KAl_2(AlSi_3O_{10})(OH)_2$	Zoisite	$Ca_2Al_3Si_3O_{12}(OH)$
Paragonite	$NaAl_2(AlSi_3O_{10})(OH)_2$		

Carrison (1966), Ringwood and Major (1967b), Sclar, Carrison, and Stewart (1967), Sclar (1970), and Yamamoto and Akimoto (1974, 1977). Reliable values of the thermodynamic properties of these minerals cannot be calculated from available experimental data, and it has yet to be demonstrated unambiguously that they are stable at high pressures and temperatures (see below).

The thermodynamic data given by Helgeson, Delany, Nesbitt and Bird (1978) for chrysotile, antigorite, and brucite lead to the conclusion that stoichiometric chrysotile is metastable with respect to the latter two phases at all pressures and temperatures. However, the Gibbs free energy and entropy changes associated with the decomposition of chrysotile to antigorite + brucite are small. As a consequence, sluggish reaction kinetics may permit early-formed metastable chrysotile to persist in metamorphic rocks. For this reason, and because slight compositional variation may stablize chrysotile relative to antigorite + brucite, alternate calculations were carried out to determine the thermodynamic consequences of the presence of chrysotile in the absence of antigorite (and vice versa) in subducting oceanic crust.

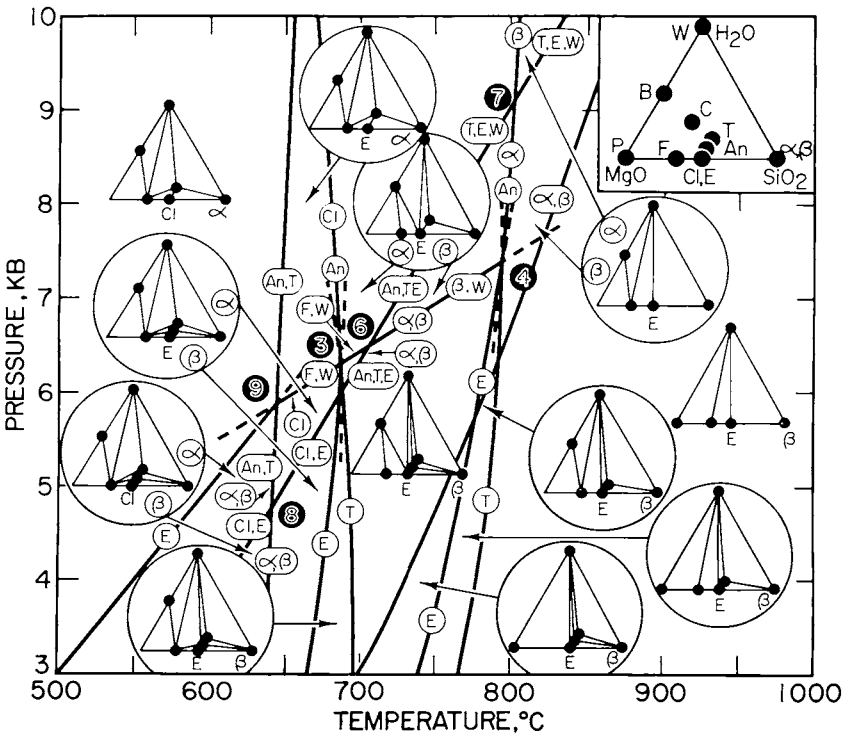

Fig. 9. Enlargement of the shaded portion of figures 7 and 8 to illustrate the relatively narrow temperature/pressure interval corresponding to the stability field of anthophyllite — see caption for figure 7.

It can be seen in figures 7 and 9 that in the absence of antigorite, humites, and the dense hydrated magnesian silicates discussed above, 13 invariant points occur in this system at pressures and temperatures from 1 bar to 100 kb and 25° to 800°C, 7 of which are at pressures > 10 kb. The pressure/temperature coordinates and phase assemblages corresponding to the invariant points are given in table 10. Note that all the low-temperature/high-pressure univariant curves are truncated by the melting curve for ice VII.

As recognized by Kitahara, Takenouchi, and Kennedy (1966), Ahrens and Schubert (1975), and others, the univariant curve representing the upper stability limit of talc is similar in configuration to the curve representing the decomposition of chrysotile, but it occurs at higher temperatures. Inspection of figures 7 and 9 reveals that these curves are separated by a 300 degree temperature interval at low pressures (below ~ 15 kb), but at 40 kb the interval decreases to ~ 150°C. The decomposition of chrysotile to talc, forsterite, and H_2O is represented in figure 7 by curve 2 *Cl*. Note in table 9 that the standard molal volume of this reaction is of the order of 40 cm^3 $mole^{-1}$ at 5 kb but decreases to zero at ~ 510°C and 17.0 kb. At higher pressures it becomes negative, reaching -7 cm^3 $mole^{-1}$ at invariant point 2. Above invariant point 2, chrysotile decomposes to forsterite, clinoenstatite, and H_2O (curve 2T). At pressures above invariant point 1, chrysotile breaks down to brucite, clinoenstatite, and H_2O.

It can be seen in figures 7 through 9 that talc decomposes to enstatite, quartz (or coesite), and H_2O only at pressures > 7.4 kb, which is also the upper pressure limit of the stability of anthophyllite.[2] The standard molal enthalpy change accompanying the decomposition of talc decreases from 16 kcal $mole^{-1}$ at the temperature extremum located at 11 kb and 805°C to 8.3 kcal $mole^{-1}$ at 40 kb and 504°C, where the volume change reaches -9.7 cm^3 $mole^{-1}$.

The effect of the breakdown of metastable chrysotile to antigorite and brucite on the relative stabilities of other mineral assemblages in the system MgO–SiO_2–H_2O can be assessed by comparing figures 7 and 8. Note that the pressure corresponding to invariant point 15 in figure 8 is ~ 10 kb higher than that of its analog (invariant point 1) in figure 7. In contrast, invariant point 14 in figure 8 (which is the analog of invariant point 2 in figure 7) occurs ~ 6 kb lower in pressure and ~ 100 degrees higher in temperature than invariant point 2. The decomposition of metastable chrysotile to antigorite, forsterite, and H_2O is represented in figure 8 by the dashed curve in the lower left corner of the diagram. The corresponding curve for the breakdown of metastable chrysotile to brucite and antigorite occurs at pressures < 1 bar.

The stability of anthophyllite in the presence of H_2O is restricted to a narrow temperature interval bounded by curves 3E and 4T in figure 9. Anthophyllite is stable in the absence of H_2O only below curve

TABLE 9

Thermodynamic properties at selected equilibrium pressures and temperatures of various univariant reactions represented by curves shown in figures 7 through 9, 11, 12, 14, 16 through 19, and 21 through 23. The invariant point numbers (IP) and the letters designating the curves correspond to those shown in the figures. The values shown in the table were computed from equations summarized above together with those given by Helgeson and Kirkham (1974) using thermodynamic data taken from Helgeson, Delany, Nesbitt, and Bird (1978).

Reaction	IP[a]	Curve[b]	Pressure[c]	Temperature[d]	ΔV°_r[e]	ΔS°_r[f]	ΔH°_r[g]
5 Chrysotile ⇌ 6 Forsterite + Talc + 9 H_2O	2	C?	5	470	39.2	112.9	83.9
			10	530	17.3	101.5	78.5
			15	584	1.4	96.0	74.7
			20	507	-5.5	91.0	70.6
Chrysotile + Brucite ⇌ 2 Forsterite + 3 H_2O	1	C?	5	391	12.1	24.1	36.3
			10	422	6.3	23.0	33.2
			20	433	-3.5	21.0	29.7
			30	413	-4.1	18.5	26.9
			40	361	-7.0	15.6	24.6
Chrysotile + Talc ⇌ 6 Clinoenstatite + 3 H_2O	2	F	25	475	-13.4	31.3	54.2
			30	420	-15.6	31.1	51.6
			40	279	-19.1	28.1	45.5
			50	85	-21.6	21.9	37.9
Talc + Forsterite ⇌ 5 Clinoenstatite + H_2O	2	C	10	668	-4.4	14.5	13.7
	15	At	15	611	-7.0	13.0	11.5
			20	540	-8.2	12.8	10.4
Talc ⇌ 3 Enstatite + Quartz + H_2O	4	An	10	803	1.3	15.0	16.2
	5	Co	15	795	-1.7	14.3	15.2
			20	775	-3.0	13.6	14.3
			25	744	-4.1	13.0	13.2
Talc ⇌ 3 Enstatite + Coesite + H_2O	5	α	30	689	-7.4	11.5	11.1
			40	504	-9.7	12.7	8.3
			50	243	-11.8	8.8	4.5
Brucite ⇌ Periclase + H_2O	11	α,3	5	756	11.8	10.7	11.0
			10	870	6.8	9.2	10.4
Antigorite ⇌ 14 Forsterite + 20 Clinoenstatite + 31 H_2O	14	T	20	588	-23.5	310.1	266.9
	15	B	30	550	-67.8	283.7	233.5
			40	475	-102.4	265.6	198.6
			50	367	-128.1	250.0	160.1
Antigorite + 14 Talc ⇌ 90 Clinoenstatite + 45 H_2O	14	F	20	571	-138.2	488.4	411.9
			30	481	-209.9	455.8	343.7
			40	352	-264.1	414.0	264.8
			50	180	-302.6	364.3	165.1

Reaction	IP[a]	Curve[b]	Pressure[c]	Temperature[d]	ΔV°_r[e]	ΔS°_r[f]	ΔH°_r[g]
Tremolite ⇌ 2 Diopside + 3 Enstatite + Quartz + H_2O			5	917	5.1	15.7	18.7
			10	927	-1.6	14.4	17.2
			15	887	-5.6	13.4	15.6
			20	828	-7.1	12.9	14.2
			25	753	-8.6	12.5	12.9
Tremolite ⇌ 2 Diopside + 3 Enstatite + Coesite + H_2O			30	651	-12.1	11.1	10.3
			35	511	-13.5	10.8	8.5
			40	347	-14.9	9.9	6.2
			45	140	-16.2	7.7	3.2
Tremolite + Forsterite ⇌ 2 Diopside + 5 Enstatite + H_2O			5	835	-1.4	14.6	16.2
			10	792	-7.8	13.4	14.3
			15	700	-11.7	13.2	12.9
			20	588	-12.4	12.1	10.4
			25	458	-13.7	12.0	8.8
			30	314	-14.7	11.4	6.7
Kaolinite + 2 α-Quartz ⇌ Pyrophyllite + H_2O	3	G	5	317	-0.2	7.6	4.5
			10	299	-1.7	6.9	4.0
			15	257	-2.6	6.8	3.6
			20	209	-2.8	6.6	3.2
2 Kaolinite ⇌ Pyrophyllite + 2 Diaspore + 2 H_2O	3	G	10	380	-2.9	10.5	6.9
			15	315	-6.5	10.1	5.9
			20	227	-8.6	9.5	4.7
Pyrophyllite + 6 Diaspore ⇌ 4 Kyanite + 4 H_2O	4	Q	10	416	12.2	55.2	38.1
	6	A	15	432	6.2	53.4	37.7
			20	443	3.5	51.6	37.3
			25	449	1.1	49.8	35.9
Pyrophyllite ⇌ Kyanite + 3 α-Quartz + H_2O	4	Co	5	447	6.5	13.3	9.6
	6	Ka	10	495	3.9	11.9	9.2
			15	517	1.7	10.8	8.6
			20	529	0.4	9.8	7.9
			25	525	-1.0	8.7	7.0
2 Diaspore + Coesite ⇌ Kyanite + H_2O	4	P	30	454	2.7	14.0	10.2
			40	498	2.4	14.1	10.8
			50	536	2.1	14.2	11.5
			60	574	2.3	14.4	12.2

TABLE 9 (continued)

Reaction	II[a]	Curve[b]	Pressure[c]	Temperature[d]	$\Delta V°_r$[e]	$\Delta S°_r$[f]	$\Delta H°_r$[g]
7A-Clinochlore ⇌ 2 Clinoenstatite + Forsterite + Spinel + 4 H_2O			5	597	23.7	45.3	38.8
			10	642	10.4	39.9	36.0
			20	653	-1.4	34.7	31.6
			30	620	-7.3	31.1	27.2
			40	541	-12.1	28.7	22.8
14A-Clinochlore ⇌ 2 Clinoenstatite + Forsterite + Spinel + 4 H_2O			70	778	-12.0	16.5	17.4
			75	683	-13.3	15.7	15..
			80	577	-14.7	15.5	13..
3 14A-Clinochlore + 5 Muscovite ⇌ 8 Kyanite + 5 Phlogopite + α-Quartz + 12 H_2O			5	603	67.9	100.0	89.3
			10	661	28.9	85.7	80..
			15	671	2.3	76.3	72.2
			20	666	-8.4	69.4	65.3
3 14A-Clinochlore + 5 Muscovite ⇌ 8 Kyanite + 5 Phlogopite + Coesite + 12 H_2O			30	593	-30.5	58.2	58.5
			35	517	-39.9	54.5	43.1
			40	418	-48.4	50.9	35.7
Paragonite + α-Quartz ⇌ Albite + Kyanite + H_2O			5	568	10.5	16.7	14..
			10	633	7.7	16.1	14.6
			15	679	5.9	15.9	15.1
			20	721	5.3	15.7	15.7
Paragonite ⇌ Jadeite + Kyanite + H_2O			20	746	-11.6	5.1	5..
			25	813	-13.7	4.0	2.8

[a]Designation of invariant points in figures 7, 8, 11, 16, 17, 19, 22, and 23. [b]Univariant curve designation in figures cited in footnote a indicating the absent phase (or phases) in the univariant assemblage (see text). [c]kb. [d]°C. [e]cm^3 $mole^{-1}$. [f]cal $mole^{-1}$ $(°K)^{-1}$. [g]kcal $mole^{-1}$.

4β,W; above 4β,W it breaks down to talc and enstatite.[2] Owing to the small entropy change accompanying the decomposition of anthophyllite to talc and enstatite, relatively large uncertainties attend calculation of the upper pressure limit of the stability of anthophyllite (Greenwood, 1971; Zen, 1971). For example, Greenwood (1963) estimated this limit to be > 20 kb from his experimental data, primarily because he failed to anticipate the strong curvature of the univariant curves representing reactions 3E, 3T, 4E, and 4T at pressures above ~ 5 kb. The dramatic changes in the Clapeyron slopes of these curves and the small entropy change accompanying reaction 4β,W are responsible for the relatively low-pressure/temperature intersections of the curves at invariant points 3 and 4. The difference in the scale of figure 9 compared to that of figures 7 and 8 affects significantly the apparent slopes of curves 3E, 3T, 4E, and 4T, all of which are nearly infinite at invariant points 3 and 4.

It can be seen in figure 7 that the Clapeyron slopes of curves 2C and 5Co are relatively small and negative above ~ 10 kb. In contrast, the slope of curve 2C computed by Essene, Wall, and Shettel (1973) and reported by Vernon (1976) is more negative, and that of 5Co more positive in the same pressure range.

Univariant curves 1C*l*, 2C*l*, 2C, and 5Co in figure 7 differ significantly from the corresponding curves determined experimentally by Kitahara, Takenouchi, and Kennedy (1966), as well as with those generated later by Kitahara and Kennedy (1967) from thermodynamic calculations. The results of these two investigations, which contradict each other, are misleading. Equilibrium was almost certainly not achieved in

[2] It should be noted in this regard that the position of the curve labeled 4β,W as well as the phase relations represented by univariant points 3 and 4 in figures 7 through 9 differ considerably from those proposed recently by Hemley and others (1977b), who generated a phase diagram with two invariant points at ~ 600°C which limit the stability of anthophyllite to pressures *above* ~ 200 to 500 bars. The latter invariant points are incompatible with the thermodynamic data summarized by Helgeson, Delany, Nesbitt, and Bird (1978), which differ from those adopted by Hemley and his coworkers.

TABLE 10

Equilibrium phase assemblages at the invariant points (IP) shown in figures 7 through 9, 11, 12, 16, 17, 19, 22, and 23.

System	IP[a]	Pressure[b]	Temperature[c]	Phases Present
$MgO-SiO_2-H_2O$	1	42.6	342	Brucite, Chrysotile, Clinoenstatite, Forsterite, H_2O
	2	22.8	495	Chrysotile, Clinoenstatite, Forsterite, Talc, H_2O
	3	6.3	687	Arthophyllite, Enstatite, Forsterite, Talc, H_2O
	4	7.4	793	Anthophyllite, β-Quartz, Enstatite, Talc, H_2O
	5	28.0	715	α-Quartz, Coesite, Enstatite, Talc, H_2O
	6	6.5	705	α-Quartz, Anthophyllite, β-Quartz, Enstatite, Talc
	7	9.1	802	α-Quartz, β-Quartz, Enstatite, Talc, H_2O
	8	4.8	642	α-Quartz, β-Quartz, Clinoenstatite, Enstatite
	9	5.9	645	Anthophyllite, Clinoenstatite, Enstatite, Talc
	10	11.1	658	Clinoenstatite, Enstatite, Forsterite, Talc, H_2O
	11	13.5	921	α-Quartz, β-Quartz, Brucite, Periclase, H_2O
	12	29.0	704	Clinoenstatite, Coesite, Enstatite, Talc, H_2O
	13	28.0	700	α-Quartz, Clinoenstatite, Coesite, Enstatite
	14	16.7	590	Antigorite, Clinoenstatite, Forsterite, Talc, H_2O
	15	51.0	355	Antigorite, Brucite, Clinoenstatite, Forsterite, H_2O
$Al_2O_3-SiO_2-H_2O$	1	21.8	210	α-Quartz, Diaspore, Gibbsite, Pyrophyllite, H_2O
	2	20.3	206	α-Quartz, Gibbsite, Kaolinite, Pyrophyllite, H_2O
	3	20.5	211	Diaspore, Gibbsite, Kaolinite, Pyrophyllite, H_2O
	4	28.7	449	Coesite, Diaspore, Kyanite, Pyrophyllite, H_2O
	5	26.2	521	α-Quartz, Coesite, Kyanite, Pyryphyllite, H_2O
	6	6.0	393	Diaspore, Kyanite, Kaolinite, Pyrophyllite, H_2O
	7	1.8	337	Andalusite, Diaspore, Kyanite, Kaolinite, Pyrophyllite
	8	2.1	357	Andalusite, Diaspore, Kyanite, Kaolinite, H_2O
	9	2.1	362	Andalusite, Kyanite, Kaolinite, Pyrophyllite, H_2O
	10	2.6	405	Andalusite, Corundum, Diaspore, Kyanite, H_2O
	11	2.8	417	Andalusite, α-Quartz, Kyanite, Pyrophyllite, H_2O
	12	3.8	497	Andalusite, Kyanite, Sillimanite
	13	23.8	208	Coesite, α-Quartz, Diaspore, Gibbsite, H_2O
	14	24.0	257	α-Quartz, Coesite, Diaspore, Pyrophyllite, H_2O

[a]Designation of invariant points in figures 7 through 9, 11, 12, 16, 17, 19, 22, and 23.
[b]Kb. [c]°C.

many of the experiments, and it can be shown (see Helgeson, Delany, Nesbitt, and Bird, 1978) that the thermodynamic data used by Kitahara and Kennedy are in error, as are a number of the assumptions they made in carrying out the calculations.

The dehydration of brucite to periclase and H_2O has been studied recently at 17, 27, and 33 kb by Irving, Huang, and Wyllie (1977). Because the equilibrium temperatures at these pressures are above 800°C, extrapolated values of $\Delta G°_{P,T,j}$ (corresponding to the dashed extensions of the curves in fig. 2) were used to compute the high-temperature portion of the brucite decomposition curve shown in figures 7 through 10. It can be seen in figure 10 that the calculated equilibrium temperature at 33 kb, which is the only pressure at which the reaction was reversed by Irving, Huang, and Wyllie, is in close agreement with the experimental data. Although the curve also agrees with their experimental data at 27 kb, there is a discrepancy of $\sim$ 50°C at 17 kb. It appears from the distribution of the curves and experimental data shown in figure 10 that the experimental observations at 17 kb are thermodynamically inconsistent with the other data reported for this reaction.

Comparison of the calculated equilibrium temperatures and pressures shown in figures 7 through 10 for the coexistence of talc, enstatite, fosterite, and H_2O, brucite, chrysotile, forsterite, and H_2O, brucite, anti-

gorite, forsterite, and H_2O, and the decomposition of chrysotile, antigorite, and talc with those reported by Yamamoto and Akimoto (1977) reveals serious discrepancies. However, none of the reactions investigated by Yamamoto and Akimoto was reversed in their experiments. Furthermore, all their experiments were of short duration (0.5-12 hrs), and in a number of instances the results contravene the phase rule. Although they report uncertainties in pressures and temperatures of ± 1 kb and ± 20° to 30°C, there can be little doubt that their overall uncertainties are much greater. For example, the data they give for the decomposition of brucite differs substantially from those obtained by Irving, Huang, and Wyllie (1977), who reversed the reaction at 33 kb. In certain instances (but not all) the experimental observations reported by Yamamoto and Akimoto (1977) agree with those given by Kitahara, Takenouchi, and Kennedy (1966), but the latter results are highly suspect (see above). It thus appears that Yamamoto and Akimoto have yet to demonstrate that they achieved equilibrium in their experiments and that the dense hydrated magnesian silicates formed in their bombs are in fact stable at high pressures and temperatures.

The system Al_2O_3–SiO_2–H_2O.—Phase relations in this system at pressures and temperatures from 1 bar to 50 kb and 25° to 600°C are shown in figures 11 and 12. The reactions corresponding to the curves are listed in table 8 together with the formulas of the minerals. It can be seen in figures 11 and 12 that 7 of the 14 invariant points that appear

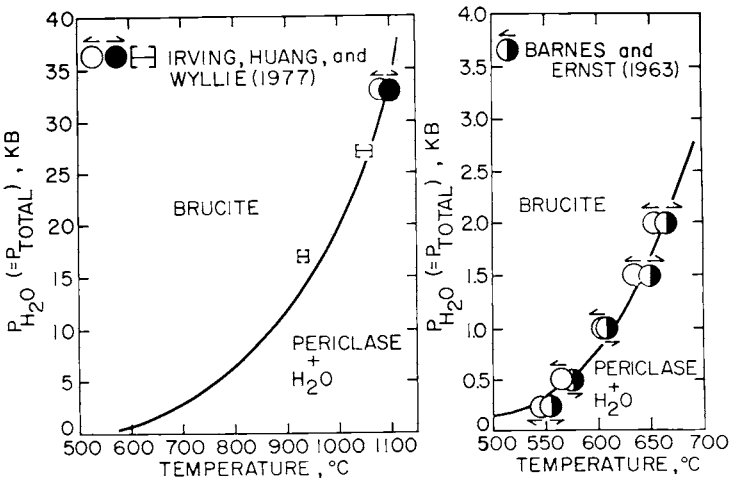

Fig. 10. Univariant curves representing the dehydration of brucite to periclase and H_2O. The symbols represent experimental data (see text), but the curves were generated from equations summarized above and those given by Helgeson and Kirkham (1974) using thermodynamic data for minerals taken from Helgeson, Delaney, Nesbitt, and Bird (1978). The arrows above the symbols indicate the direction from which equilibrium was approached in the experiments. The filled circles represent complete conversion of brucite to periclase and H_2O, but the open circles indicate the reverse reaction.

in the diagrams occur at pressures > 10 kb. The coordinates of the invariant points and the corresponding phase assemblages are given in table 10.

Because the standard molal entropies of reaction are small for the decomposition of kaolinite to gibbsite and pyrophyllite, and the breakdown of pyrophyllite to diaspore and quartz (curves 2W and 1G,W in fig. 11), considerable uncertainty attends calculation of equilibrium pressures and temperatures for these reactions. Consequently, the phase relations shown in figure 11 for temperatures $\lesssim$ 300°C may differ significantly from those in geologic systems. Nevertheless, they afford a basis for approximating the thermodynamic consequences of the dehydration of kaolinite and pyrophyllite in the sediment cover of subducting oceanic crust.

The upper stability limit of gibbsite is represented in figure 11 by the curve labeled P,Ka, and α,Co, which passes through invariant points 1, 3, and 13. The standard molal volume of the reaction, gibbsite $\rightleftharpoons$ diaspore + H_2O decreases from 2 cm^3 mole^{-1} at low pressures to ~ zero at invariant point 3. The curves labeled 2G and 3G in figure 11, which represent the coexistence of kaolinite, quartz, pyrophyllite, and H_2O, and

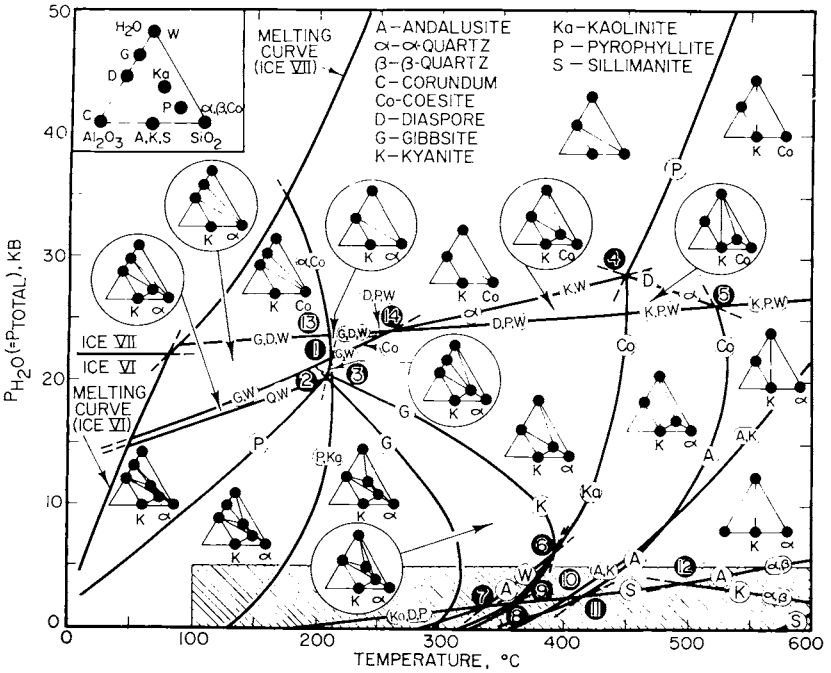

Fig. 11. Equilibrium phase relations in the system Al_2O_3–SiO_2–H_2O generated from equations summarized above and those given by Helgeson and Kirkham (1974) using thermodynamic data for minerals taken from Helgeson, Delany, Nesbitt, and Bird (1978) — see caption for figure 7. The shaded portion of the figure is enlarged in figure 12.

kaolinite, diaspore, pyrophyllite, and H_2O, respectively, exhibit positive Clapeyron slopes at low pressures, which become negative before they terminate at invariant points 2 and 3.

The stability field of pyrohyllite is bounded at low temperatures by the reaction, pyrophyllite $\rightleftharpoons$ 2 diaspore + 4 quartz (curve 1G,W). At invariant point 14, the quartz/coesite transition limits the pressure at which pyrophyllite is stable between invariant points 4 and 14. The slope of curve 14α is small because the standard molal entropy and volume changes accompanying the transition of quartz to coesite are ~ -0.5 cal mole^{-1} (°K)$^{-1}$ and ~ -2 cm^3 mole^{-1}, respectively. The quartz/coesite transition has a similar effect on the decomposition of pyrophyllite to kyanite, quartz, and H_2O, which is represented by curve 5Co. As a result, curve 4P (which corresponds to 2 diaspore + coesite $\rightleftharpoons$ kyanite + H_2O) is the only univariant curve that extends to pressures > 29 kb at temperatures > 200°C.

The difficulties involved in both experimental and thermodynamic investigation of phase relations in the system Al_2O_3–SiO_2–H_2O at both high temperatures and low pressures and low temperatures and high pressures are underscored by the small sizes of many of the stability fields shown in figures 11 and 12. The configurations of curves 2G, 3G, 6Ka, and 5Co in figure 11 are similar at low pressures to those computed by Wall and Essene (1972) and reported by Vernon (1976) but depart significantly at high pressures. For example, Wall and Essene located an invariant point corresponding to the coexistence of pyrophyllite, kaolinite, diaspore, quartz, and H_2O near 5 kb and 310°C, but the present calculations suggest this is a metastable assemblage. Also, their invariant

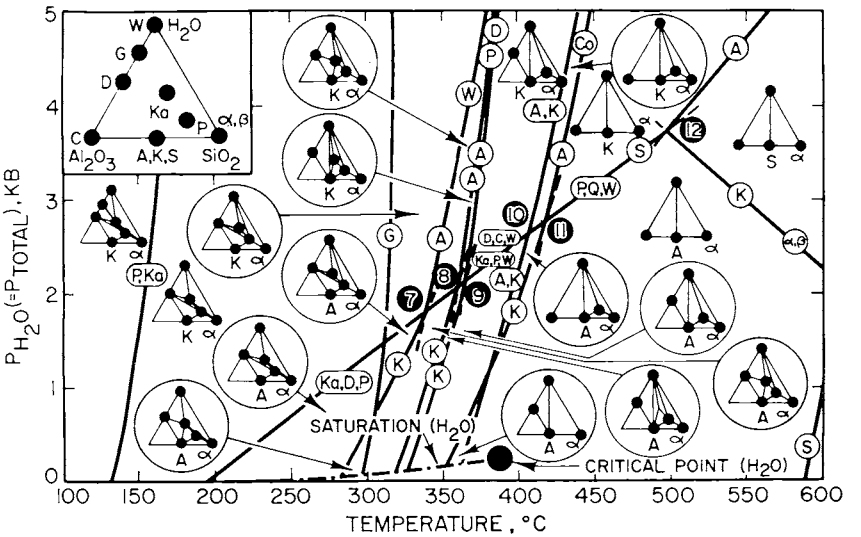

Fig. 12. Enlargement of the shaded portion of figure 11 to illustrate the consequences of the kyanite/andalusite transition — see caption for figure 11.

points 4 and 5 are ~ 100°C higher than the temperature shown for these points in figure 11 and table 10.

High-pressure experimental data for the reactions gibbsite $\rightleftharpoons$ diaspore + H_2O and 2 diaspore $\rightleftharpoons$ corundum + H_2O (Kennedy, 1959) are shown in figure 13. It can be seen that the curve representing the decomposition of gibbsite agrees reasonably well with the experimental data at 10 and 20 kb but not at higher pressures. However, because this reaction was not reversed experimentally, there is no evidence that Kennedy achieved equilibrium.

The cause of the obvious discrepancy between the computed curve in figure 13 representing diaspore $\rightleftharpoons$ corundum + H_2O and the experimental data reported by Kennedy (1959) is not clear. Kennedy's high-pressure experiments were performed with a piston-anvil type device. In a later publication (Kitahara and Kennedy, 1964), he compared the results of experiments using piston-anvil equipment and hydrothermal apparatus for a number of reactions and concluded that his early experiments using the piston-anvil device yielded results that were assigned to too high a pressure. If a pressure correction were applied to Kennedy's data for the reaction of diaspore to give corundum and H_2O in figure 13, it would move his data points in the direction of the curve generated from thermodynamic calculations. Comparative thermodynamic analysis indicates that the Clapeyron slope of a curve passing through Kennedy's data points would be ~ 400 bars $(°K)^{-1}$ at 30 kb, compared to 147 bars $(°K)^{-1}$ for the curve generated in the present study. Resolution of such a large discrepancy would require the computed standard molal volume or entropy of H_2O to be in error by as much as 3 cm^3 $mole^{-1}$ or 30 cal $mole^{-1}$ $(°K)^{-1}$, respectively, at 30 kb and 660°C. It can be seen in figures 4, 5, and 6 that such errors exceed by far uncertainties in the regression calculations for H_2O reported above. Kennedy's data are also

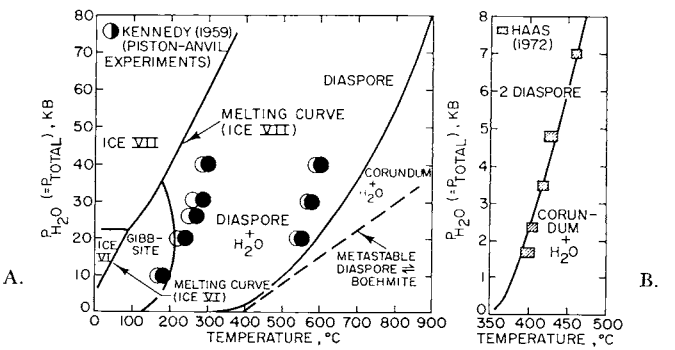

Fig. 13. Univariant phase relations in the system Al_2O_3–H_2O. The symbols represent experimental data, but the curves were generated from equations summarized above and those given by Helgeson and Kirkham (1974) using thermodynamic data taken from Helgeson, Delany, Nesbitt, and Bird (1978). The hatched symbols designate reversed reaction intervals, but the other symbols represent conversion of gibbsite to diaspore or corundum.

thermodynamically inconsistent with those obtained by Haas (1972) at low pressures as well as with the metastable equilibrium curve for diaspore/boehmite shown in figure 13.

Univariant reactions in the system CaO–MgO–SiO_2–H_2O.—The reaction of tremolite + forsterite to give diopside, clinoenstatite or enstatite, and H_2O, and the decomposition of tremolite to diopside, clinoenstatite or enstatite, α-quartz, β-quartz, or coesite, and H_2O are represented by univariant curves shown in figure 14. It can be seen that these curves exhibit pronounced curvature and reversal in sign of their Clapeyron slopes at pressures below 10 kb, which agrees with the results of Essene, Wall, and Shettel's (1973) calculations as reported by Vernon (1976). With increasing pressure and decreasing temperature, the first of these reactions is characterized by slightly smaller standard molal enthalpies and entropies of reaction (table 9). The volume changes for these reactions become more negative with increasing pressure and reach −13.7 and −8.6 cm^3 $mole^{-1}$ at 25 kb, which correspond to 5 and 3 percent, respectively, of the volume of the reactants.

The invariant point labeled A in figure 14 actually represents three invariant points that occur so close to one another that they cannot be shown with clarity on the diagram. The assemblages corresponding to the invariant points are: tremolite, diopside, clinoenstatite, coesite, enstatite, H_2O; coesite, α-quartz, clinoenstatite, enstatite; tremolite, diopside, enstatite, coesite, α-quartz, H_2O.

DEHYDRATION REACTIONS IN SUBDUCTING OCEANIC CRUST

Correlation of the thermodynamic calculations summarized above to processes occurring in the upper mantle requires a model for the tem-

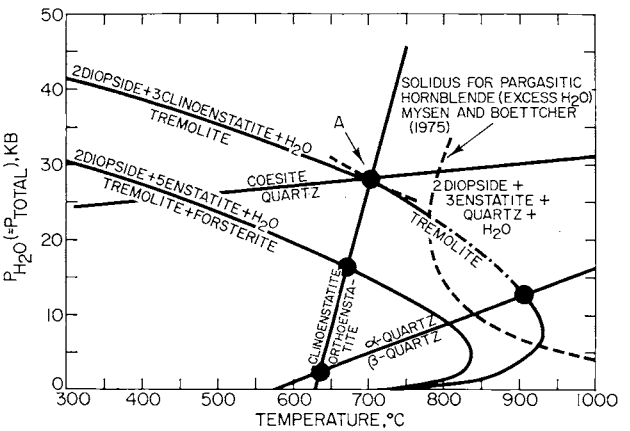

Fig. 14. Univariant curves and invariant points representing equilibrium among minerals in the system CaO–MgO–SiO_2–H_2O generated from equations summarized above and those given by Helgeson and Kirkham (1974) using data taken from Helgeson, Delany, Nesbitt, and Bird (1978). The dashed curves correspond to metastable extensions, but the dash-dot curve is interpolated. See text for explanation of invariant point A.

perature/depth distribution in subducting plates. Many such models have been proposed in recent years, but few take into account dehydration equilibria.

Thermal models of descending plates.—Distinctions among various thermal models of subducting lithosphere arise from the extent to which they provide for radiogenic heating, adiabatic compression, phase changes, frictional (shear strain) heating, and other variables such as the angle and rate of descent, thickness of the plate, thermal conductivity of the rock, et cetera. Of the thermal profiles shown in figure 15, only curve H is based solely on a steady-state frictional heat balance (Oxburgh and Turcotte, 1970). It can be seen that this curve, which corresponds to the thermal profile along the leading edge at the top of the plate, intersects the experimental solidus for gabbro with excess H_2O at 6 kb. Consequently, the model proposed by Oxburgh and Turcotte (1970) would require melting in subduction zones at far shallower depths than is generally believed to be the case.

In contrast to Oxburgh and Turcotte (1970), Toksöz, Minear, and Julian (1971) considered all the mechanisms of heat generation cited above in a series of calculations in which they varied the heat source term. The results of two of these calculations are represented by curves F and G in figure 15. Curve F was generated by providing for the olivine/spinel and spinel/post-spinel phase changes at 350 and 600 to 700 km, respectively. Curve G differs only in that provision for the latter phase change was omitted, which strongly affects the computed temperature/depth distribution in the slab. The model adopted by Schubert, Yuen, and Turcotte (1975) represented by curve E also provides for both phase

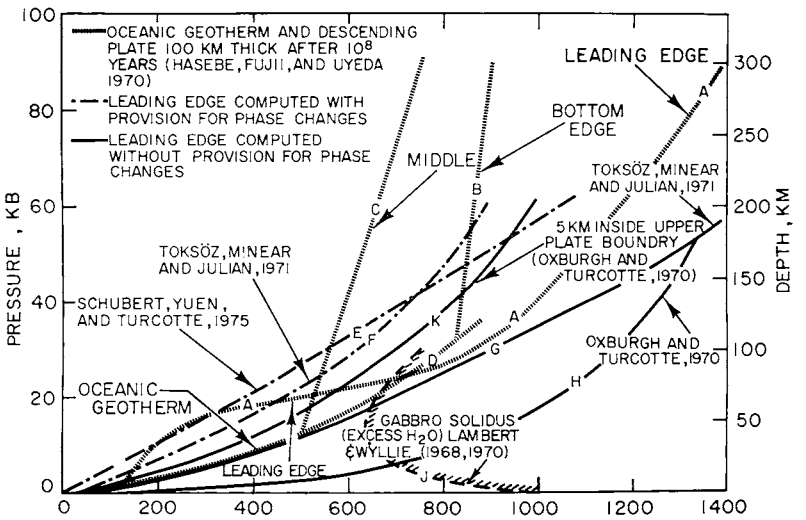

Fig. 15. Temperature/pressure/depth distribution in descending plates computed from various thermal models (see text).

changes, but in addition takes account of convection in a fluid layer at depth.

Curves A through C in figure 15 were generated from a model developed by Hasebe, Fujii, and Uyeda (1970) from observations of heat flow and seismicity in the Sea of Japan. To account for the heat flow measurements, they omitted provision in their model for frictional heating at depths < 60 km, which resulted in much lower computed temperatures at pressures < 25 kb than those calculated by Toksöz, Minear, and Julian (1971) represented by curve G. Although curve A satisfies heat flow observations in the Sea of Japan, as emphasized by Hasebe, Fujii, and Uyeda (1970), the agreement is not necessarily a consequence of the absence of frictional heating in the upper 60 km of the plate. They suggest that dehydration might well account for the heat flow observations, which is consistent qualitatively with conclusions reached in the present study. Note that the thermal profile representing the middle of the plate (curve C) departs from the oceanic geotherm at about 13 kb and 500°C with a gradient of only 1°C km^{-1}. The middle of the plate remains cooler than the leading edge of the plate as long as the rate of descent of the downgoing slab is greater than ~ 5 cm year^{-1} (Toksöz, Minear, and Julian, 1971). The temperature distribution at the base of the oceanic crust computed by Oxburgh and Turcotte (1970) is also shown in figure 15 (curve K).

Although significantly different thermal profiles result from different models of subduction zones, any one of the curves in figure 15 represent-

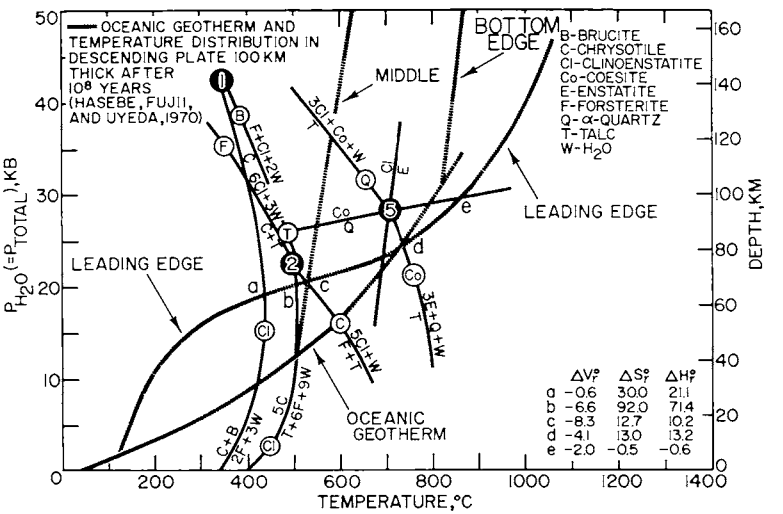

Fig. 16. Calculated temperature/pressure/depth distribution of univariant curves (figs. 7 and 9) and thermal profiles (fig. 15) in a subduction zone (see text). The standard molal enthalpies, entropies, and volumes of reaction shown for the intersections of univariant curves with the leading edge of the plate are expressed in kcal mole^{-1}, cal mole^{-1} (°K)$^{-1}$, and cm^3 mole^{-1}, respectively. The circled numbers and letters indicate invariant points and univariant curves — see caption for figure 7.

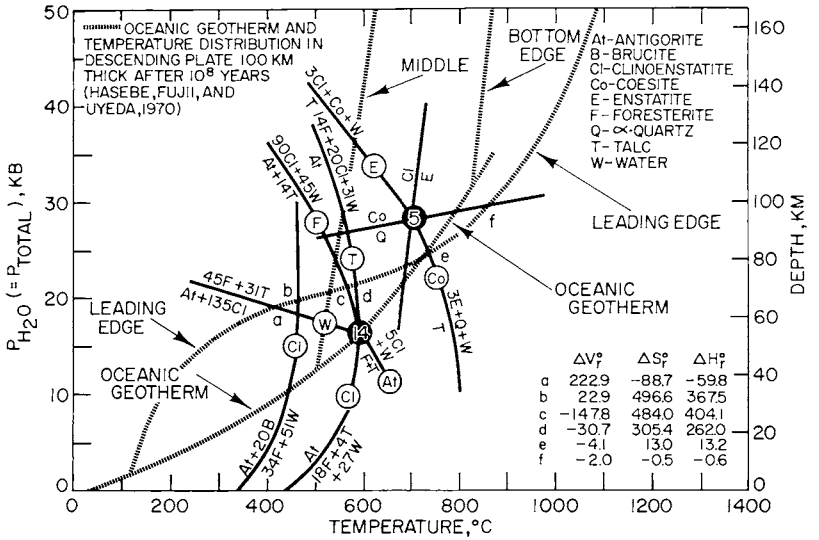

Fig. 17. Calculated temperature/pressure/depth distribution of univariant curves (figs. 8 and 9) and thermal profiles (fig. 15) in a subduction zone (see text and caption for fig. 16).

ing the leading edge of the subducting plate can be used to illustrate the general thermodynamic consequences of dehydration in descending oceanic crust. Only the absolute depths at which the reactions occur will vary from model to model. Because the leading edge profile computed by Hasebe, Fujii, and Uyeda (1970) is most consistent with dehydration in the upper part of subduction zones, curve A was used in the present study to calculate the depth distribution of the reaction fronts discussed below.

Thermodynamic considerations.—Intersections of univariant curves generated above (figs. 7 through 9, 11, 12, and 14) with the leading edge of the descending plate modeled by Hasebe, Fujii, and Uyeda (1970) are shown in figures 16 through 19. The intersections are labeled with lower case letters. It can be seen that 11 of the curves representing equilibria in the system $CaO–MgO–SiO_2–H_2O$ cross the leading edge in the relatively narrow depth interval from ~ 60 to 80 km. The thermodynamic properties shown in figures 16 and 18 for these reactions at the leading edge of the plate indicate that the disappearance of chrysotile, talc, and tremolite results in a volume decrease of 1.4 percent for chrysotile and 3 percent each for talc and tremolite. In contrast, the corresponding enthalpy changes for the latter two reactions at the leading edge (13.2 and 12.9 kcal $mole^{-1}$, respectively) are slightly smaller than that required to cause the decomposition of one mole of chrysotile (14.3 kcal $mole^{-1}$). However, because chrysotile contains 2 moles of H_2O, the enthalpy change (mole $H_2O)^{-1}$ associated with the breakdown of chrysotile is approximately half that required to liberate one mole of H_2O by the decomposi-

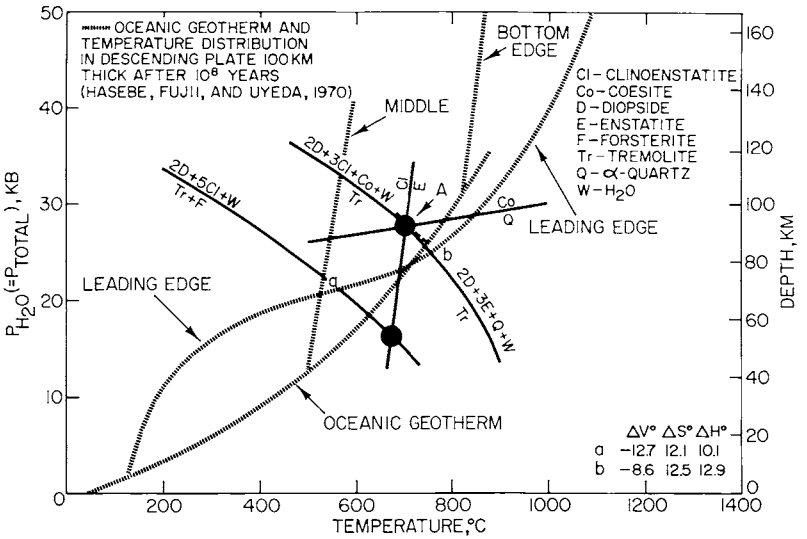

Fig. 18. Calculated temperature/pressure/depth distribution of univariant curves (fig. 14) and thermal profiles (fig. 15) in a subduction zone — see text and caption for figure 16.

tion of either talc or tremolite. Similarly, the volume decrease (mole $H_2O)^{-1}$ caused by the disappearance of chrysotile is about a quarter of that associated with liberation of one mole of H_2O by the dehydration of talc or tremolite. It can be deduced from figure 17 that the decomposition of antigorite to forsterite, clinoenstatite, and H_2O at the leading edge of the plate requires ~8.5 kcal (mole $H_2O)^{-1}$, and the volume change accompanying the reaction is −1 cm^3 (mole $H_2O)^{-1}$.

Although Anderson, Uyeda, and Miyashiro (1976) argue that dehydration reactions act as a heat sink and control to a large extent the heat distribution below dehydration fronts in subduction zones, it appears likely that the extent to which these reactions proceed is a function of the rate at which heat generated by other processes is transmitted through the slab to the dehydration reaction fronts, relative to the subduction rate. It can be shown that an average subduction rate of 5 cm yr^{-1} requires a minimum heat flow of 1.4 microcal cm^{-2} sec^{-1} to convert 20 wt percent[3] tremolite at the leading edge of the subducting crust to diopside, enstatite, and quartz. Because heat flow at depth in subduction zones is considerably greater than this (Hasebe, Fujii, and Uyeda, 1970), it seems likely that any tremolite in the descending crust will break down completely in the absence of kinetic barriers. However, heat flow calculations also indicate that 3.2 and 4.7 microcal cm^{-2} sec^{-1}, respectively,

[3] Although the actual abundance of tremolite, talc, and chrysotile in subducting oceanic crust is highly uncertain, the figure of 20 wt percent serves to illustrate the order of magnitude of the heat required to convert hydrous phases to their anhydrous counterparts in descending slabs.

are required for equilibrium decomposition of 20 wt percent[3] talc or chrysotile at the leading edge of a plate subducting at a rate of 5 cm yr^{-1}. These values are close to that estimated by Hasebe, Fujii, and Uyeda to be the average heat flow into a slab descending at a rate of 3 cm yr^{-1} (4.4 microcal cm^{-2} sec^{-1}). Nevertheless, because the magnitude of the heat flow into downgoing slabs is a function of the temperature distribution in the slabs as well as the angle and rate of descent, it appears that under certain conditions the relatively large endothermic enthalpies of dehydration (unit mass)$^{-1}$ required for the breakdown of talc and chrysotile may lead to persistence of these phases at depths below those corresponding to their equilibrium decomposition temperatures.

Although the calculations described above pertain only to stoichiometric phases, they afford insight into the thermodynamic requirements for dehydration of amphiboles and serpentines in general. For example, estimated thermodynamic properties and equilibrium temperatures and pressures for the decomposition of ferrotremolite as well as actinolite solid solutions at high pressures and temperatures yield results similar to those discussed above for tremolite. For reactions with negative Clapeyron slopes, solid solution in hydrous minerals increases univariant equilibrium temperatures and pressures, but only if the effects of compositional variation in the hydrous minerals are not offset by solid solution among the product phases. Because solid dehydration products commonly exhibit solid solution, the high-pressure equilibrium temperatures computed above are probably maximal.

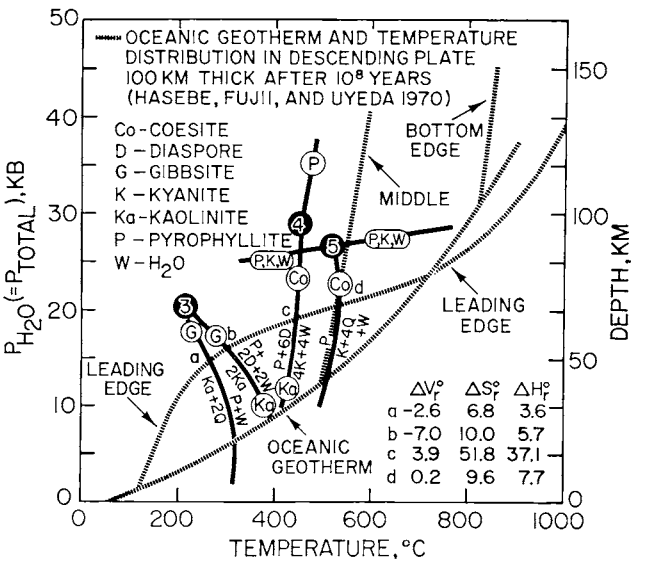

Fig. 19. Calculated temperature/pressure/depth distribution of univariant curves (figs. 11 and 12) and thermal profiles (fig. 15) in a subduction zone — see text and caption for figure 16.

Several curves representing equilibria in the system Al_2O_3–SiO_2–H_2O are shown in figure 19. It can be seen that the intersections of the univariant curves with the leading edge of the descending plate (denoted by points *a* through *d*) occur at lower pressures and temperatures than the analogous intersections in figures 16 through 18. Nevertheless, the general configurations of the curves are similar. As emphasized above, the relevance of mineral equilibria in the system Al_2O_3–SiO_2–H_2O to subduction processes is probably restricted to reactions in the sediment cover of the ocean floor. However, the extent to which minerals in this system are incorporated into the actual material being subducted is a subject of considerable debate (see Church, 1973; Church and Tilton, 1973; Coleman, 1973; Ringwood, 1974; Scholl and Marlow, 1974; Karig and Sharman, 1975).

Univariant equilibria at high pressures and temperatures are depicted in figures 20 and 21 for a large number of calcium, potassium, and sodium aluminosilicates. The equilibrium temperatures and pressures defined by the curves shown in these figures were computed in the manner described above. It can be deduced from figures 20 and 21 that plagioclase is unstable with respect to grossular, kyanite, jadeite, and quartz (or coesite) at pressures $>$ 10 to $\sim$ 30 kb, which correspond to depths of 30 to 100 km. Note that neither the curve representing the reaction of albite with quartz to form jadeite, nor that corresponding to the breakdown of anorthite to grossular, kyanite, and quartz intersects the leading edge of the plate defined by Hasebe, Fujii, and Uyeda's (1970) model.

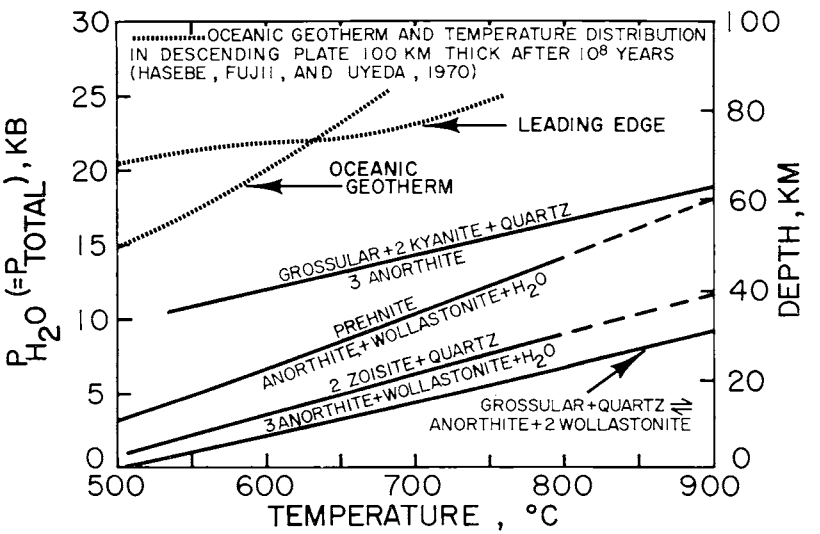

Fig. 20. Calculated temperature/pressure/depth distribution of univariant curves representing equilibrium among phases in the system CaO–Al_2O_3–SiO_2–H_2O and thermal profiles (fig. 15) in a subduction zone (see text). Extrapolations are shown by dashed curves.

Both the entropy and volume changes accompanying these reactions are positive.

Of the four micas considered in the present study (muscovite, paragonite, phlogopite, and annite), only paragonite is unstable at high pressures. It can be seen in figure 21 that the univariant curves representing equilibria involving paragonite terminate in an invariant point at 20.5 kb and 725°C. Paragonite decomposes to jadeite, kyanite, and H_2O at pressures between ~ 20 and 30 kb. The univariant curve for this reaction intersects the leading edge of the plate at ~ 22 kb and 615°C (point *a* in fig. 21), where the volume and enthalpy changes accompanying the reaction are -12.5 cm^3 mole^{-1} and 4.2 kcal mole^{-1}, respectively. At the intersection of the univariant curve with the leading edge, the heat flow required for 5 wt percent paragonite to decompose to jadeite,

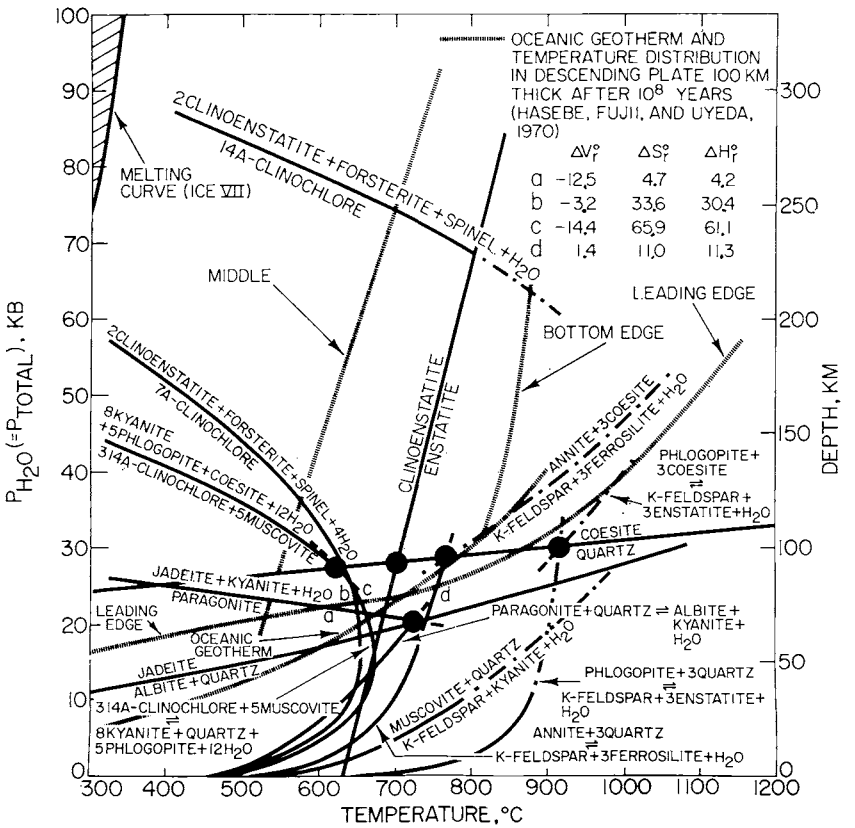

Fig. 21. Calculated temperature/pressure/depth distribution of univariant curves representing equilibrium among minerals in the system K_2O–Na_2O–MgO–FeO–Al_2O_3–SiO_2–H_2O and thermal profiles (fig. 15) in a subduction zone — see text and caption for figure 16. Invariant points are represented by filled circles and extrapolations are shown by dot-dash curves.

kyanite, and H_2O at a subduction rate of 5 cm year^{-1} is only 0.2 microcal cm^{-2} sec^{-1}.

In general, whether or not a given dehydration curve exhibits a temperature maximum is controlled by the extent to which the sum of the standard molal volumes of the product minerals ($V°_p$) differs from that of the reactants ($V°_r$). If $V°_r$ exceeds $V°_p$ by less than 10 to 14 cm^3 mole^{-1}, the curve will not exhibit an extremum. However, in the case of the univariant curves in figure 21 representing the reaction of annite and phlogopite with quartz to produce feldspar and pyroxene, the fact that the curves fail to exhibit negative Clapeyron slopes at high pressures is caused by the quartz/coesite transition, rather than the relative size of $V°_r$ and $V°_p$. The small negative entropy and relatively large negative volume changes associated with the quartz/coesite transition are responsible for the abrupt positive shift in the slopes of the curves above the transition. Note that annite as well as muscovite, phlogopite, and biotite solid solutions almost certainly melt at depth before they dehydrate.

Because chlorite is a common mineral in greenschist assemblages, the univariant curves representing the decomposition of 7A and 14A clinochlore in figure 21 are particularly relevant to geochemical processes in subducting oceanic crust. Although 7A-clinochlore is apparently metastable at all pressures and temperatures (Helgeson, Delany, Nesbitt, and Bird, 1977), chlorite formed at temperatures below ~ 500°C is almost invariably of the 7A variety. The points labeled *b* and *c* in figure 21 refer to the intersection of the leading edge of the plate with the univariant curves representing the decomposition of 7A-clinochlore and the reaction of 14A-clinochlore with muscovite to give phlogopite, kyanite, quartz, and H_2O. It can be seen that these intersections (at ~ 22.5 kb and 635° and 650°C, respectively) occur in the same relatively narrow depth interval as 11 of the intersections in figures 16 through 18. The thermodynamic properties shown in figure 21 indicate that the decomposition of 7A-clinochlore is accompanied by an enthalpy change which is about half that associated with the reaction of 14A-clinochlore with muscovite. Note that a relatively large negative volume change (mole of clinochlore)$^{-1}$ accompanies both these reactions. It should also be emphasized that the calculations reported above indicate that 14A-clinochlore may persist in subducting oceanic crust well into the mantle, which is in agreement with conclusions reached recently by Staudigel and Schreyer (1977). It can be deduced from figure 21 that 14A-clinochlore almost certainly melts before it decomposes. In contrast, metastable 7A-clinochlore should tend to break down to 14A-clinochlore or (at higher pressures and temperatures) to clinoenstatite, forsterite, and spinel above ~ 20 to 25 kb.

A number of the univariant curves discussed above are shown in the cartoons of a descending plate in figures 22 and 23, where it can be seen that the equilibrium reaction fronts represented by the curves follow the general configuration of the isotherms computed by Hasebe, Fujii, and Uyeda (1970). All the reaction fronts depicted in the cartoons,

as well as several involving 7A-clinochlore (which were omitted for the sake of clarity) cross the oceanic crust at depths ranging from 60 to 100 km. In contrast to figures 16 through 19 and 21, the thermodynamic properties of dehydration reactions shown in the cartoons are expressed (mole H_2O released)$^{-1}$ at the leading edge of the plate. It can be seen that $\Delta V°_r$ and $\Delta H°_r$ range from 0.2 to 8.6 cm^3 and 7.0 to 13.2 kcal (mole H_2O released)$^{-1}$.

Owing to the configurations of the isotherms in figures 22 and 23, invariant points 2 and 14 occur at the leading edge as well as the middle of the plate. Note that invariant point 14 is also intersected by the oceanic geotherm. The geologic significance of the replication of these invariant points in the middle of the plate depends on the depth to which hydrothermal alteration of the upper mantle takes place as the plate moves from the spreading center toward the continental margin. If deep circulation of convecting interstitial seawater near spreading centers produces hydrous phases well below the crust/mantle boundary, the exothermic nature of the reactions as well as subsequent endothermic dehydration during subduction may affect significantly the distribution of heat in the middle of the plate. It can be seen in figures 22 and 23 that if tremolite and talc are present in the upper part of subducting

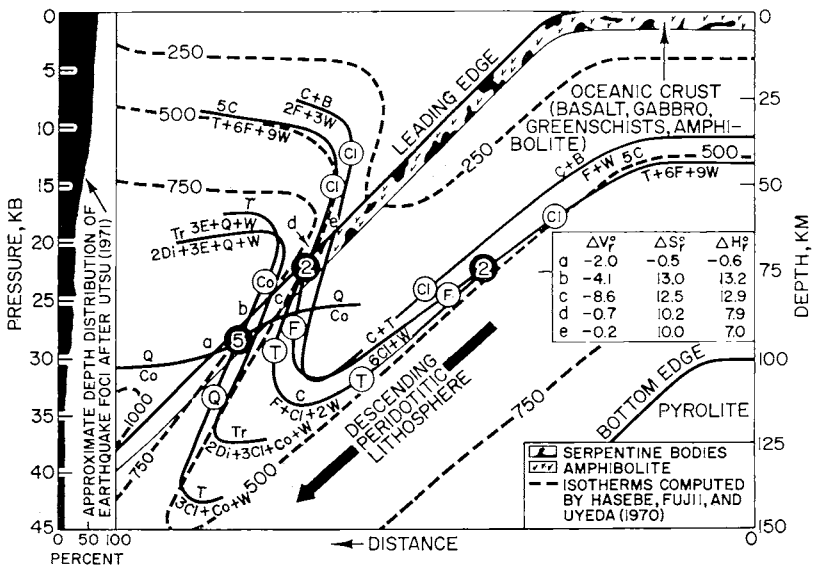

Fig. 22. Cartoon of a subducting plate modified after Hasebe, Fujii, and Uyeda (1970) and Ringwood (1974) with superimposed invariant points and univariant curves taken from figures 7 and 14 (see text). Except for the quartz/coesite transition, the standard molal enthalpy, entropy, and volume changes shown for the intersections of univariant curves with leading edge of the plate are expressed in kcal (mole H_2O released)$^{-1}$, cal (mole H_2O released)$^{-1}$ (°K)$^{-1}$, and cm^3 (mole H_2O released)$^{-1}$, respectively.

mantle material, they may persist to depths as great as 125 and 140 km, respectively.

Focal mechanism solutions for earthquakes indicate tensional stress fields in the upper parts of descending slabs (Evison, 1967; Isaacks and Molnar, 1971; Toksöz, Sleep, and Smith, 1973; and others) which may result from the relatively large negative volume changes accompanying dehydration of minerals at depth. The distribution of earthquakes shown on the left of figures 22 and 23 is consistent with this observation. If earthquakes can be attributed in part to phase changes as suggested by Griggs (1972), Ringwood (1972, 1973), Vaisnys and Pilbeam (1976), and others, it appears likely from the calculations carried out in the present study that those in the upper part of the subduction zone may well be caused by tensional stress fields induced in part by dehydration reactions at depth. However, as observed by Greenwood (1976, written commun.) direct coupling of dehydration reactions and earthquake propagation is probably not realistic because it would require reaction rates approaching P-wave velocities.

CONCLUDING REMARKS

Although subject to various uncertainties arising from ambiguities in the volumetric response of minerals to increasing pressure and temperature, the calculations summarized above afford a reasonable first approximation of the thermodynamic consequences of dehydration reactions in

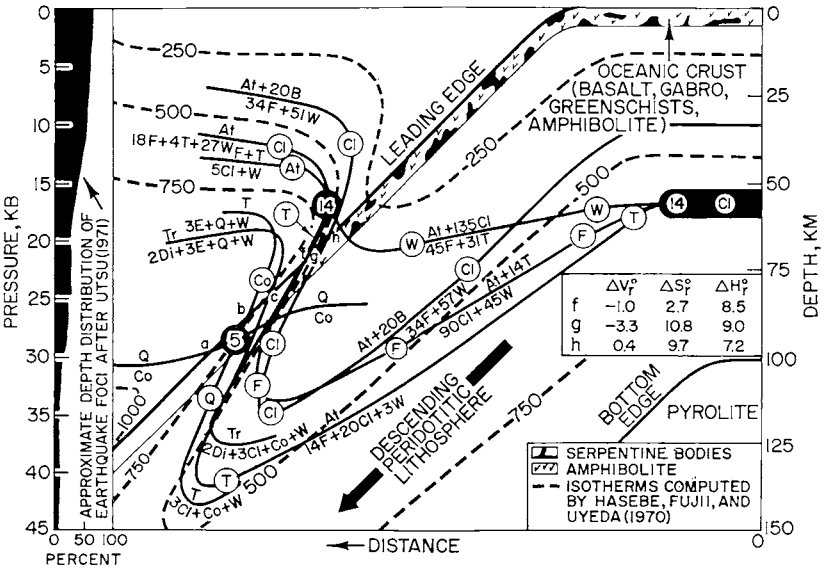

Fig. 23. Cartoon of a subducting plate modified after Hasebe, Fujii, and Uyeda (1970) and Ringwood (1974) with superimposed invariant points and univariant curves taken from figures 8 and 14 — see caption for figure 22. Points a through c are the same as those shown in figure 22.

subducting lithosphere. As such, they provide the means to incorporate quantitative provision for such reactions in thermal models of descending plates. Because the endothermic enthalpy changes accompanying dehydration reactions are much larger than those for solid/solid reactions, it appears likely that revision of thermal models to incorporate explicitly the effects of dehydration will alter significantly the various geotherms shown in figure 15.

The present study leaves little doubt that volume changes accompanying dehydration reactions may contribute significantly to earthquake generation at continental margins. They also indicate that 14A-chlorite as well as muscovite and biotite may persist at depth in subduction zones, where they may constitute potential reservoirs of volatiles for geochemical processes in the mantle. Quantitative consideration of these and other factors discussed above would seem to be a requisite for future development of more realistic tectonic models of descending plates.

Further work is required to investigate the extent to which differences in fluid and rock composition and subduction rates affect the thermodynamic consequences of dehydration processes. In some instances, liberation of H_2O may depress the thermal regime and inhibit melting. In others, the high fugacity of H_2O may accelerate reaction rates and induce melting of the crust. These processes depend in part on the extent to which mixed volatiles and solid solution affect dehydration/decarbonation reactions in subducting plates. In some cases these effects are probably negligible, but in others they are almost certainly of first-order importance.

Although the calculations reported above are consistent with Ringwood's (1974) petrogenetic model of subduction zones, it appears that eclogites formed by progressive metamorphism are stable only at much higher pressures than those commonly assigned to these rocks. The calculations carried out in the present study suggest that the petrogenetic models of subducting plates and high-pressure metamorphic facies, such as those proposed by Allen (1972), Ahrens and Schubert (1975), Turner (1968), Winkler (1974), and others, are in need of revision.

ACKNOWLEDGMENTS

The research reported in this paper was carried out in partial fulfillment of the requirements for the senior author's Master of Science degree at the University of California, Berkeley. We are indebted to Lane Johnson, Tom McEvilly, John Walther, David Kirkham, Philip Behrman, Per Aagaard, Dennis Bird, George Flowers, William McKenzie, Mike Lee, Joachim Hampel, Titus Boleslawski, Richard Lloyd, Karen Bailey, Debbie Aoki, Terri Brooks, and others among our friends and colleagues at Berkeley for helpful suggestions and assistance during the course of this study. Various aspects of the research were supported by the National Science Foundation under the auspices of NSF Grants GA 25314, GA 36023, GA 35888, and DES 74-14280, together with the donors of the Petroleum Research Fund administrated by the American

Chemical Society under PRF Grant 5356-AC2. Thanks are also due the Committee on Research and the Miller Institute at the University of California, Berkeley, who supported one of us (HCH) as a Miller Professor for the academic year 1975. Finally, we would like to express our appreciation to H. J. Greenwood, T. J. Ahrens, P. M. Orville, J. Verhoogen, J. Holloway, and J. Wood for their constructive reviews of the manuscript and helpful suggestions for improvement.

References

Ahrens, T. J., and Schubert, G., 1975, Gabbro–eclogite reaction rate and its geophysical significance: Rev. Geophysics Space Physics, v. 13, p. 383-400.

Akimoto, S., and Fujisawa, H., 1968, Olivine–spinel solid solution equilibria in the system Mg_2SiO_4–Fe_2SiO_4: Jour. Geophys. Research, v. 73, p. 1467-1479.

Allen, J. C., Modreski, P. J., Haygood, C., and Boettcher, A. L., 1972, The role of water in the mantle of the earth: The stability of amphiboles and micas: Internat. Geol. Cong., 24th, Montreal 1972, sec. 2, p. 231-240.

Anderson, A. T., 1975, Some basaltic and andesitic gases: Rev. Geophysics Space Physics, v. 13, p. 37-56.

Anderson, G. M., and Burnham, C. W., 1965, The solubility of quartz in supercritical water: Am. Jour. Sci., v. 263, p. 494-511.

Anderson, R. N., Uyeda, S., and Miyashiro, A., 1976, Geophysical and geochemical constraints at converging plate boundaries, Part 1, Dehydration in the downgoing slab: Royal Astron. Soc. Jour., v. 44, p. 333-357.

Barnes, H. L., and Ernst, W. G., 1963, Ideality and ionization in hydrothermal fluids, the system MgO–H_2O–NaOH: Am. Jour. Sci., v. 261, p. 129-150.

Benson, S. W., 1968, Thermochemical kinetics: New York, John Wiley & Sons, 223 p.

Birch, F., 1966, Compressibility; Elastic constants, *in* Clark, S. P., Jr., ed., Handbook of Physical Constants: Geol. Soc. America Mem. 97, p. 97-173.

Bridgman, P. W., 1942, Freezing parameters and compressions of twenty-one substances to 50,000 $Kgkm^2$: Am. Acad. Arts and Sci. Proc., v. 74, p. 399-424.

Brown, A. J., and Whalley, E., 1966, Preliminary investigation of the phase boundaries between ice VI and VII and ice VI and VIII: Jour. Chem. Physics, v. 45, p. 4360-4361.

Burnham, C. W., Holloway, J. R., and Davis, N. F., 1969, Thermodynamic properties of water to 1,000°C and 10,000 bars: Geol. Soc. America Spec. Paper 132, 96 p.

Burte, A. S., and Nicholson, P. S., 1972, Influence of anisotropy and water vapor on the solid state reaction of CaO and beta quartz: Am. Ceramic Soc. Jour., v. 55, p. 472.

Cameron, M., Sueno, S., Prewitt, C. T., and Papike, J. J., 1973, High-temperature crystal chemistry of acmite, diopside, hedenbergite, jadeite, spodumene, and ureyite: Am. Mineralogist, v. 58, p. 594-618.

Chen, C. H., and Presnall, D. C., 1975, The system Mg_2SiO_4–SiO_2 at pressures up to 25 kb: Am. Mineralogist, v. 60, p. 398-406.

Christensen, N. I., 1970a, Composition and evolution of the oceanic crust: Marine Geology, v. 8, p. 139-154.

———— 1970b, Possible greenschist facies metamorphism of the oceanic crust: Geol. Soc. America Bull., v. 81, p. 905-908.

———— 1972, Abundance of serpentinites in the oceanic crust: Jour. Geology, v. 80, p. 709-718.

Church, S. E., 1973, Limits of sediment involvement in the genesis of orogenic volcanic rocks: Contr. Mineralogy Petrology, v. 39, p. 17-32.

Church, S. E., and Tilton, G. R., 1973, Lead and strontium isotopic studies in the Cascade Mountains: Bearing on andesite genesis: Geol. Soc. America Bull., v. 84, p. 431-454.

Coleman, P. J., ed., 1973, The western Pacific island arcs, marginal seas and geochemistry: Nedlands Univ. Western Australia Press, p. 569-601.

Demarest, H. H., Jr., 1972, Lattice model calculation of elastic and thermodynamic properties at high pressure and temperature: Physics Earth Planetary Interiors, v. 6, p. 146-153.

Eggler, D. H., 1976, Does CO_2 cause partial melting in the low velocity layer of the mantle: Geology, v. 4, p. 69-72.

Essene, E. J., Hensen, B. J., and Green, D. H., 1970, Experimental study of amphibolite and eclogite stability: Physics Earth Planetary Interiors, v. 3, p. 378-384.

Essene, E. J., Wall, J. J., and Shettel, D., 1973, Equilibria in $CaO–MgO–SiO_2–H_2O$: Am. Geophys. Union Trans., v. 54, p. 480.

Evison, F. F., 1967, On the occurrence of volume change at the earthquake source: Seismolog. Soc. America Bull., v. 57, p. 9-25.

Finger, L. W., and Ohashi, Y., 1976, The thermal expansion of diopside to 800°C and a refinement of the crystal structure at 700°C: Am. Mineralogist, v. 60, p. 303-310.

Fyfe, W. S., and McBirney, A. R., 1975, Subduction and the structure of andesitic volcanic belts: Am. Jour. Sci., v. 275-A, p. 285-297.

Giardini, A. A., Hurst, V. J., Melton, C. E., and Stormer, J. C., Jr., 1974, Biotite as a primary inclusion in diamond: its nature and significance: Am. Mineralogist, v. 59, p. 783-789.

Goldsmith, J. R., and Newton, R. C., 1974, An experimental determination of the alkali feldspar solvus, *in* MacKenzie, W. S. and Zussman, J., eds., The Feldspars: NATO Adv. Study Inst. Proc., Manchester Univ. Press, p. 337-359.

Green, D. H., 1973, Experimental melting studies on a model upper mantle composition at high pressures under water-saturated conditions: Earth Planetary Sci. Letters, v. 19, p. 37-53.

Green, D. H., and Ringwood, A. E., 1967a, An experimental investigation of the gabbro to eclogite transformation and its petrological significance: Geochim. et Cosmochim. Acta, v. 31, p. 767-833.

———— 1967b, The genesis of the calcalkaline igneous rock suite: Contr. Mineralogy Petrology, v. 15, p. 103-190.

Green, H. W., 1972, A CO_2 charged atmosphere: Nature, v. 238, p. 2-5.

Green, H. W., and Radcliffe, S. W., 1975, Fluid precipitates in rocks from the earths mantle: Geol. Soc. America Bull., v. 86, p. 846-852.

Greenwood, H. J., 1963, The synthesis and stability of anthophyllite: Jour. Petrology, v. 4, p. 317-351.

———— 1971, Anthophyllite. Corrections and comments on its stability: Am. Jour. Sci., v. 270, p. 151-154.

Griggs, D. T., 1972, The sinking lithosphere and the focal mechanisms of deep earthquakes, *in* Robertson, E. C., ed., The Nature of the Solid Earth: New York, McGraw-Hill, p. 361-384.

Haas, H., 1972, Diaspore–corundum equilibrium determined by epitaxis of diaspore on corundum: Am. Mineralogist, v. 57, p. 1375-1385.

Hasebe, K., Fujii, N., and Uyeda, S., 1970, Thermal processes under island arcs: Tectonophysics, v. 10, p. 335-355.

Helgeson, H. C., 1969, Thermodynamics of hydrothermal systems at elevated temperatures and pressures: Am. Jour. Sci., v. 267, p. 729-804.

Helgeson, H. C., Delany, J. M., Nesbitt, H. W., and Bird, D. K., 1978, Summary and critique of the thermodynamic properties of rock-forming minerals: Am. Jour. Sci., v. 278-A, in press.

Helgeson, H. C., and Kirkham, D. H., 1974, Theoretical prediction of the thermodynamic behavior of aqueous electrolytes at high pressures and temperatures: 1. Summary of the thermodynamic/electrostatic properties of the solvent: Am. Jour. Sci., v. 274, p. 1089-1198.

———— 1976, Theoretical prediction of the thermodynamic behavior of aqueous electrolytes at high pressures and temperatures: III. Equation of state for aqueous species at infinite dilution: Am. Jour. Sci., v. 276, p. 97-240.

Hemley, J. J., 1959, Some mineralogical equilibria in the system $K_2O–Al_2O_3–SiO_2–H_2O$: Am. Jour. Sci., v. 257, p. 241-270.

Hemley, J. J., Meyer, C., and Richter, D. H., 1961, Some alteration reactions in the system $Na_2O–Al_2O_3–SiO_2–H_2O$: U.S. Geol. Survey Prof. Paper 424D, p. 338-340.

Hemley, J. J., Montoya, J. W., Christ, C. L., and Hostetler, P. B., 1977a, Mineral equilibria in the $MgO–SiO_2–H_2O$ system: I. Talc–chrysotile–forsterite–brucite stability relations: Am. Jour. Sci., v. 277, p. 322-351.

Hemley, J. J., Montoya, J. W., Nigrini, A., and Vincent, H. A., 1971, Some alteration reactions in the system $CaO–Al_2O_3–SiO_2–H_2O$: Mining Geol. Soc. Japan Spec. Issue, v. 2, p. 58-63.

Hemley, J. J., Montoya, J. W., Shaw, D. R., and Luce, R. W., 1977b, Mineral equilibria in the MgO–SiO_2–H_2O system: II. Talc–antigorite–forsterite–anthophyllite–enstatite stability relations and some geologic implications in the systems: Am. Jour. Sci., v. 277, p. 353-383.

Hill, R. E. T., and Boettcher, A. L., 1970, Water in the earth's mantle: melting curves of basalt-water and basalt-water-carbon dioxide: Science, v. 167, p. 980-982.

Howard, J. C., 1961, Thermodynamic data for water: Washington, D.C., U.S. Dept. Commerce, Office Tech. Services, 15 p.

Huang, W. L., and Wyllie, P. J., 1973, Muscovite dehydration and melting in deep crust and subducted oceanic sediments: Earth Planetary Sci. Letters, v. 18, p. 133-136.

———— 1975, Melting and subsolidus phase relationships for $CaSiO_3$ to 35 kilobars pressure: Am. Mineralogist, v. 60, p. 213-217.

Irving, A. J., Huang, W. L., and Wyllie, P. J., 1977, Phase relations of portlandite, $Ca(OH)_2$ and brucite, $Mg(OH)_2$ to 33 kilobars: Am. Jour. Sci., v. 277, p. 313-321.

Isaacks, B., and Molnar, P., 1971, Distribution of stresses in the descending lithosphere from a global survey of focal mechanisms solutions of mantle earthquakes: Rev. Geophysics Space Physics, v. 9, p. 103-174.

Jüza, J., 1966, An equation of state for water and steam, steam tables in the critical region and in the range from 1,000 to 100,000 bars: Rozprav. Ceskoslovenske Akad. VED. Rada TV, v. 76, p. 3-121.

Karig, D. E., and Sharman, G. F., 1975, Subduction and accretion in trenches: Geol. Soc. America Bull., v. 86, p. 277-389.

Keenan, J. H., Keyes, F. G., Hill, P. G., and Moore, J. G., 1969, Steam tables: New York, John Wiley & Sons, Inc., 162 p.

Kelley, K. K., 1960, Contributions to the data on theoretical metallurgy XIII. High-temperature heat-content, heat capacity, and entropy data for the elements and inorganic compounds: U.S. Bureau Mines, Bull. 584, 232 p.

Kennedy, G. C., 1959, Phase relations in the system Al_2O_3–H_2O at high temperatures and pressures: Am. Jour. Sci., v. 257, p. 563-573.

Kennedy, G. C., and Holser, W. T., 1966, Pressure-volume-temperature and phase relations of water and carbon dioxide, *in* Clark, S. P., Jr., ed., Handbook of Physical Constants: Geol. Soc. America Mem. 97, p. 371-383.

Kitahara, S., and Kennedy, G. C., 1964, The quartz–coesite transition: Jour. Geophys. Research, v. 69, p. 5395-5400.

———— 1967, The calculated equilibrium curves for some reactions in the system MgO–SiO_2–H_2O at pressures up to 30 kilobars: Am. Jour. Sci., v. 265, p. 211-217.

Kitahara, S., Takenouchi, S., and Kennedy, G. C., 1966, Phase relations in the system MgO–SiO_2–H_2O at high temperatures and pressures: Am. Jour. Sci., v. 264, p. 223-233.

Kushiro, I., 1970, Systems bearing on melting of the upper mantle under hydrous conditions: Carnegie Inst. Washington Year Book 68, p. 240.

Kushiro, I., Syono, Y., Akimoto, S., 1967, Stability of phlogopite at high pressures and the possible presence of phlogopite in the earth's upper mantle: Earth Planetary Sci. Letters, v. 3, p. 197-203.

Lambert, I. B., and Wyllie, P. J., 1968, Stability of hornblende and a model for the low velocity zone: Nature, v. 219, p. 1240-1241.

———— 1970a, Melting in the deep crust and upper mantle and the nature of the low velocity layer: Physics Earth Planetary Interiors, v. 3, p. 316-322.

———— 1970b, Low velocity zone of the earth's mantle: Incipient melting caused by water: Science, v. 169, p. 764-766.

Melson, W. G., Thompson, G., and van Andel, J. A., 1968, Volcanism metamorphism in the mid-Atlantic ridge, 22°N latitude: Jour. Geophys. Research, v. 73, p. 5925-5941.

Melton, C. E., and Giardini, A. A., 1975, Experimental results and theoretical interpretations of gaseous inclusions in Arkansas natural diamonds: Am. Mineralogist, v. 60, p. 413-417.

Ming, L. C., and Bassett, W. A., 1975, The post-spinel phases in the Mg_2SiO_4–Fe_2SiO_4 system: Science, v. 187, p. 66-68.

Miyashiro, A., 1973, Metamorphism and metamorphic belts: New York, Halsted Press, 492 p.

Morey, G. W., 1957, The solubility of solids in gases: Econ. Geology, v. 52, p. 225-251.

Morey, G. W., and Hesselgesser, J. M., 1951, The solubility of some minerals in superheated steam at high pressures: Econ. Geology, v. 46, p. 821-835.

Mysen, B. O., and Boettcher, A. L., 1975, Melting of a hydrous mantle: 1. Phase relations of natural peridote at high pressures and temperatures with controlled activities of water, carbon dioxide, and hydrogen: Jour. Petrology, v. 16, p. 520-548.

Mysen, B. O., Eggler, D. H., Seitz, M. G., and Holloway, J. R., 1976, Carbon dioxide in silicate melts and crystals. Part 1. Solubility measurements: Am. Jour. Sci., v. 276, p. 455-479.

Nicholls, I. A., and Ringwood, A. E., 1973a, Production of silica-saturated tholeiitic magmas in island arcs: Earth Planetary Sci. Letters, v. 17, p. 243-246.

———— 1973b, Effect of water on olivine stability in tholeiites and the production of silica-saturated magmas in the island arc environment: Jour. Geology, v. 81, p. 285-300.

Orville, P. M., 1963, Alkali ion exchange between vapor and feldspar phases: Am. Jour. Sci., v. 261, p. 201-237.

———— 1972, Plagioclase cation exchange equilibria with aqueous chloride solution: results at 700°C and 2000 bars in the presence of quartz: Am. Jour. Sci., v. 272, p. 234-272.

Oxburgh, E. R., and Turcotte, D. L., 1970, Thermal structure of island arcs: Geol. Soc. America Bull., v. 81, p. 1665-1688.

Pistorius, C. W. F. T., 1963a, Thermal decomposition of portlandite and xonotlite to high pressures and temperatures: Am. Jour. Sci., v. 261, p. 79-87.

———— 1963b, Some phase relations in the system $MgO–SiO_2–H_2O$ at high pressures and temperatures: Neues Jahrb. Mineralogie Monatsh, v. 11, p. 283-293.

Pistorius, C. W. F. T., and Sharp, W. E., 1960, Properties of water. Part VI. Entropy and Gibbs free energy of water in the range of 10-1000°C and 1-250,000 bars: Am. Jour. Sci., v. 258, p. 757-768.

———— 1961, Erratum — Properties of water. Part VI. Entropy and Gibbs free energy of water in the range 10-1,000°C and 1-250,000 bars, a clarification: Am. Jour. Sci., v. 259, p. 397-398.

Pistorius, C. W. F. T., Pistorius, M. C., Blakey, J. P., and Admiraal, L. J., 1963, Melting curve of ice VII to 200 kbar: Jour. Chem. Physics, v. 38, p. 600-602.

Poty, B. P., and Stalder, H. A., 1970, Kryometrische Bestimmungen der Salz. und. Gasgehalte eingeschlossener Lössungen in Quarzkristallen aus Zerrklüften der Schweizer Alpen, Schweiz: Schweizer min. pet. Mitt., v. 50, p. 141-154 [English abs.].

Poty, B. P., Stalder, H. A., and Weisbroad, A. M., 1974, Fluid inclusion studies in quartz from fissures of western and central Alps: Schweizer min. pet Mitt., v. 54, p. 717-752.

Rice, M. H., and Walsh, J. M., 1957, Equation of state of water to 250 kb: Jour. Chem. Physics, v. 26, p. 824-830.

Ringwood, A. E., 1972, Phase transformations and mantle dynamics: Earth Planetary Sci. Letters, v. 14, p. 233-241.

———— 1973, Phase transformations and their bearing on the dynamics of the mantle: Forsch. Mineralogie, v. 50, p. 113-139.

———— 1974, The petrological evolution of island arc systems: Geol. Soc. London, v. 130, p. 183-204.

———— 1975, Composition and petrology of the earth's mantle: San Francisco, McGraw-Hill, 618 p.

Ringwood, A. E., and Major, A., 1967a, Some high pressure transformations of geophysical interest: Earth Planetary Sci. Letters, v. 2, p. 106-110.

———— 1967b, High pressure reconnaissance investigation in the system Mg_2SiO_4–$MgO–H_2O$: Earth Planetary Sci. Letters, v. 2, p. 130-133.

Robie, R. A., and Waldbaum, D. R., 1968, Thermodynamic properties of minerals and related substances at 298.15°K (25°C) and one atmosphere (1.013 bars) pressure and at higher temperatures: U.S. Geol. Survey Bull. 1259, 256 p.

Roedder, E., 1965, Liquid CO_2 inclusions in olivine bearing nodules and phenocrysts from basalts: Am. Mineralogist, v. 50, p. 1746-1783.

———— 1972, Composition of fluid inclusions: Chapter JJ of Fleischer, M., ed., Data of Geochemistry: U.S. Geol. Survey Prof. Paper 440-JJ, 164 p.

Scholl, D. W., and Marlow, M. S., 1974, Sedimentary sequences in modern Pacific trenches and the deformed eugeosyncline: Soc. Econ. Paleontologists Mineralogists Spec. Paper 19, p. 193-211.

Sclar, C. B., 1970, High pressure studies in the system $MgO–SiO_2–H_2O$: Physics Earth Planetary Interiors, v. 3, p. 333.

Sclar, C. B., and Carrison, L., 1966, High-pressure reactions and shear strength of serpentinized dunite: Science, v. 153, p. 1285-1286.

Sclar, C. B., Carrison, L. C., and Stewart, O. M., 1967, High pressure synthesis of a new hydroxylated pyroxene in the system $MgO–SiO_2–H_2O$ [abs.]: Am. Geophys. Union Trans., v. 48, p. 226.

Sclar, C. B., and Schwartz, C. M., 1964, High-pressure stability field of clinoenstatite and the orthoenstatite–clinoenstatite transition [abs.]: Am. Geophys. Union Trans., v. 45, p. 121.

———— 1965, High pressure synthesis and stability of a new hydronium-bearing layer silicate in the system $MgO–SiO_2–H_2O$ [abs.]: Am. Geophys. Union Trans., v. 46, p. 184.

Schreinemakers, F. A. H., 1916, In-, mono- and divariant equilibria: Amsterdam Acad. Sci. Proc., v. 18, p. 820-828.

Schubert, G., Yuen, D. A., and Turcotte, D. L., 1975, Role of phase transitions in a dynamic mantle: Royal Astron. Soc. Geophys. Jour., v. 42, p. 705-735.

Sharp, W. E., 1962, The thermodynamic functions for water in the range −10 to 1000°C and 1 to 250,000 bars: Livermore, Calif., Univ. California Lawrence Radiation Lab., UCRL-7118, 51 p.

Simmons, G., and Wang, H., 1971, Single crystal elastic constants and calculated aggregate properties: A Handbook: Cambridge, Mass., M.I.T. Press, 370 p.

Skinner, B. J., 1966, Thermal expansion, *in* Clark, S. P., Jr., ed., Handbook of Physical Constants: Geol. Soc. America Mem. 97, p. 75-96.

Spetzler, H., 1970, Equation of state of polycrystalline and single crystal MgO to 8 kilobars and 800 K: Jour. Geophys. Research, v. 75, p. 2073-2087.

Spetzler, H., Sammis, C. G., and O'Connell, R. J., 1972, Equation of state of NaCl: Ultrasonic measurements to 8 kbar and 800°C and static lattice theory: Jour. Phys. Chemistry Solids, v. 33, p. 1727-1750.

Spooner, E. T. C., and Fyfe, W. S., 1973, Sub-sea floor metamorphism, heat and mass transfer: Contr. Mineralogy Petrology, v. 42, p. 287-304.

Staudigel, H., and Schreyer, W., 1977, The upper thermal stability of clinochlore, $Mg_5Al(AlSi_3O_{10})(OH)_8$, at 10-35 kb P_{H_2O}: Contr. Mineralogy Petrology, v. 61, p. 181-198.

Sueno, S., Cameron, M., Papike, J. J., and Prewitt, C. T., 1973, The high temperature crystal chemistry of tremolite: Am. Mineralogist, v. 58, p. 649-664.

Tödheide, K., 1972, Water at high temperatures and pressures, *in* Franks, F., ed., Water, v. I: New York, Plenum Press, p. 463-514.

Toksöz, M. N., Minear, J. W., and Julian, B. R., 1971, Temperature field and geophysical effects of a downgoing slab: Jour. Geophys. Research, v. 76, p. 1113-1138.

Toksöz, M. N., Sleep, N. H., and Smith, A. T., 1973, Evolution of the down-going lithosphere and the mechanisms of deep focus earthquakes: Royal Astron. Soc. Geophys. Jour., v. 35, p. 285-310.

Tourét, J., 1971a, Le facies granulite en Norvege Meridionale I. Les associations mineralogiques: Lithos, v. 4, p. 239-249 [English abs.].

———— 1971b, Les facies granulite en Norvege Meridoionale II. Les inclusions fluids: Lithos, v. 4, p. 423-436 [English abs.].

———— 1974, Fluid inclusions in high grade metamorphic rocks, NATO Advanced Studies Institute "Volatiles in metamorphism": Nancy, France, 36 p.

Turner, F. J., 1968, Metamorphic petrology: San Francisco, McGraw-Hill, 403 p.

Utsu, T., 1971, Seismological evidence for anomalous structure of island arcs with special reference to the Japanese region: Rev. Geophysics Space Physics, v. 9, p. 839-890.

Vaisnys, J. R., and Pilbeam, C. C., 1976, Deep-earthquake initiation by phase transformation: Jour. Geophys. Research, v. 81, p. 985-988.

Vernon, R. H., 1976, Metamorphism processes: London, George Allen and Unwin, 247 p.

Wagman, D. D., Evans, W. H., Harlow, I., Parker, V. B., Bailey, S. M., and Schumm, R. H., 1968, Selected values of chemical thermodynamic properties, pt. 3: Natl. Bur. Std. Tech. Note 270-3, 264 p.

Wall, J. J. ,and Essene, E. J., 1972, Subsolidus equilibria in $CaO–Al_2O_3–SiO_2–H_2O$: Geol. Soc. America Abs. with Programs, v. 4, p. 700.

Walsh, J. M., and Rice, M. H., 1957, Dynamic compression of liquids from measurements on strong shock waves: Jour. Chem. Physics, v. 26, p. 815-823.

Weill, D. F., and Fyfe, W. S., 1964, The solubility of quartz in H_2O in the range 1000-4000 bars and 400-500°C: Geochim. et Cosmochim. Acta, v. 28, p. 1243-1255.

Winkler, H. G. F., 1974, Petrogenesis of metamorphic rocks: New York, Springer-Verlag, 320 p.

Wolery, T. J., and Sleep, N. H., 1976, Hydrothermal circulation and geochemical flux at mid-ocean ridges: Jour. Geology, v. 84, p. 249-275.

Wyllie, P. J., 1970, Ultramafic rocks and the upper mantle: Mineralog. Soc. America Spec. Paper 3, p. 3-32.

———— 1971, The dynamic earth: textbook in geosciences: New York, John Wiley & Sons, p. 63-90.

———— 1973, Experimental petrology and global tectonics — A preview: Tectonophysics, v. 17, p. 189-209.

Wyllie, P. J., and Huang, W. L., 1976, Carbonation and melting reactions in the system $CaO–MgO–SiO_2–CO_2$ at mantle pressures with geophysical and petrological applications: Contr. Mineralogy Petrology, v. 54, p. 79-107.

Yamamoto, K., and Akimoto, S., 1974, High pressure and high temperature investigations in the system $MgO–SiO_2–H_2O$: Jour. Solid State Chemistry, v. 9, p. 187-195.

———— 1977, The system $MgO–SiO_2–H_2O$ at high pressures and temperatures-stability field for hydroxyl–chondrodite, hydroxyl–clinohumite, and 10 Å-phase: Am. Jour. Sci., v. 277, p. 288-312.

Yamaoka, S., Fukunaga, O., and Saito, S., 1970, Phase equilibrium in the system $MgO–H_2O$ at high temperatures and very high pressures: Am. Ceramics Soc. Jour., v. 53, p. 179-181.

Zen, E-an, 1966, Construction of pressure-temperature diagrams for multi-component systems after the method of Schreinemakers — a geometric approach: U.S. Geol. Survey Bull. 1225, 56 p.

———— 1971, Comments on the thermodynamic constants and hydrothermal stability relations of anthophyllite: Am. Jour. Sci., v. 270, p. 136-150.